Summer Course on Process and Device Modelling
ESAT Leuven-Heverlee, Belgium, June 7-10, 1983

MOS MODELLING AT LOW CURRENT DENSITY

by H.J. Oguey and S. Cserveny
Centre Electronique Horloger S.A., Neuchâtel, Switzerland

SUMMARY

The low current static characteristics of MOSFETs are based on both drift and diffusion carrier transport. The long channel approximation of Pao and Sah gives an accurate implicit formulation of the current in an ideal situation. Modelling of this ideal case by an explicit system of equations is discussed and extended to real situations by a review of the most important effects, including mobility variation, non uniform doping, weak inversion, medium and short channels.

The adequacy and limits of this model are compared with other approaches in particular with two-dimensional simulations, and with experiments.

LIST OF SYMBOLS

a_h	parameter in f_h
a_w	parameter in f_w
b_h	parameter in f_h
b_w	parameter in f_w
B	effective gain defined by (64)
B_o	effective gain at low field defined by (65)
B_2	normalized body factor defined by (16)
C_D	depletion layer capacitance per unit area
C_{ox}	oxide capacitance per unit area
C_{ss}	surface state capacitance per unit area
C_w	parameter in f_w
d_{ox}	oxide thickness
D_I	implanted dose
D_n	electron diffusion coefficient
E	electric field
E_C	critical field at which carriers reach saturation velocity
f_h	strong inversion function defined by (46 and 47)
f_w	weak inversion function defined by (29 and 31)
F	charge sharing factor
F_1	normalized total charge density defined by (9)
F_2	auxiliary function $F_2 = F_1 \exp(-u_F/2)$
F_3	normalized mobile charge defined by (14)
I	channel current
I_{sat}	saturation current
I_T	normalization factor for currents defined by (15)
K	body factor defined by (23)
K_w	weak inversion parameter (see Appendix I)
ℓ_{dep}	length of the depletion region between channel and drain
L	layout channel length
L_o	effective channel length before saturation
L_B	extrinsic Debye length for background doping before ion implantation
L_D	intrinsic Debye length

m	subthreshold parameter defined by (70)
n	subthreshold parameter defined by (71)
n	electron concentration
n_i	intrinsic carrier density
N_B	bulk doping concentration
T	absolute temperature
u	normalized potentials or voltages defined by (2)
u_C	normalized control voltage defined by (26)
u_D	normalized drain voltage
u_{Dsat}	normalized drain saturation voltage
u_F	normalized equilibrium Fermi potential defined by (3)
u'_G	normalized gate voltage defined by (19)
u_h	parameter in f_h
u_m	normalized surface potential at threshold
u_{sD}	normalized surface potential at the drain
u_{sS}	normalized surface potantial at the source
u_S	normalized source to substrate voltage
u_{surf}	normalized surface potential
U_{TH}	thermodynamic potential kT/q
V	voltages
V_C	control voltage
V_D	drain to substrate voltage
V_D^*	expression corresponding to V_D limited at V_{Dsat} (see p. 21)
V_{Dsat}	drain to substrate saturation voltage
V_{FB}	flat-band voltage
V_G	gate to substrate voltage
V_S	source to substrate voltage
V_T	threshold voltage
V_{TO}	threshold voltage for $V_S = 0$
W	layout channel width
W_o	effective channel width
x	distance into substrate from Si-SiO_2 interface
x_C	distance from the surface of the centroid of the depleted portion of the implanted dose
x_i	inversion layer depth
y	distance along the channel from the source
y	normalized current component

γ	function defined by (27)
ε_{ox}	permittivity of SiO_2
ε_S	permittivity of Si
η	parameter used to fit the transition formula (56)
Θ	parameter for mobility degradation due to the transversal field
λ_1	coefficient for ℓ_{dep} adjustment used in (62)
λ_2	coefficient for mobile charge effect adjustment in ℓ_{dep} used in(62)
μ	effective channel carrier mobility
μ_o	low field channel carrier mobility
ξ	normalized difference between electron and hole quasi-Fermi potantiels
ρ	charge density
ϕ	potentials
ϕ_F	bulk Fermi potential

1. Introduction

Progress in the field of Very Large Scale Integration rests heavily on computer simulation. As MOSFETs play a central role in VLSI, a realistic simulation calls for adequate models. The broad field of VLSI can be divided into three categories, where quite different modeling philosophies are required:

1. Device optimization concentrates on a detailed analysis of device properties, especially of small devices. This is the domain of two- and three- dimensional simulations. Here, the long time necessary to obtain a single simulation is of secundary importance.
2. Digital system simulation, on the other hand, has to consider a limited number of situations (on-off), requires a limited accuracy, but needs a very simple analytical formulation of device properties in order to make possible the simulation of a complex system.
3. Analog circuit simulation lies in-between. It needs an accurate model of the MOSFET, valid in a wide range of situations (with respect to dimensions and currents), but still a simple analytical formulation of active devices and parasitic effects, compatible with computer simulation of complex analog circuits.

Consequently, there is no such thing as an universal MOSFET model, but more of a hierarchy of models, each presenting the proper trade-off between complexity on one side, accuracy and range of validity on the other side.

Today, most CAD programs in the categories 2 and 3 still include MOSFET models of limited validity. Weak inversion effects are poorly formulated, sometimes even ignored.

On the other hand, the operation of many circuits is critically dependent upon low level currents, and their optimization should rest on a valid formulation. A few examples of such circuits are easy to find: dynamic memories, low power digital and analog circuits for watches, pocket instruments, implanted medical electronics, switched capacitor filters and A/D converters for telecommunications, etc...

This paper concentrates on the low-current description of MOSFETs and on extensions of known models with a view to obtain an explicit and accurate formulation of the dc characteristics, valid in a wide range of voltages and currents. It starts with the long channel integral expression of Pao and Sah. Approximate explicit relations are proposed, valid in weak inversion, in strong inversion and, by an interpolation formula, also in the transition region; they are adjusted to fit with numerical solutions. The next step is a discussion of the most important deviations from the ideal situation, and of extension of the equations. The complete model finally is compared with two-dimensional simulations and with measurements.

2. The long channel model

Conduction in MOSFETs for gate voltages above threshold is controlled mainly by drift in a very narrow region called the channel. Under this channel area, we find a depleted region of the substrate which has to be taken into account in order to describe correctly the so called bulk effect.

For gate voltages slightly below threshold, the semiconductor is in weak inversion. Carrier transport takes place mainly by diffusion and is responsible for the small current observed under this condition.

Pao and Sah [66 Pa] presented the first analysis combining both drift and diffusion currents. Despite the fact that this paper has been widely commented in textbooks [69 Sz, 78 Mu, 81 Br], we will base our discussion mainly on the original paper.

2.1 Hypotheses about the physical structure

A classical idealized MOSFET structure is assumed (Fig. 1). In a p-type silicon substrate, two highly n-doped regions form the source and the drain. They are separated from the substrate (bulk) by abrupt junctions. The channel zone has a length L_o and a width W_o. Above it is an oxide of thickness d_{ox} and a gate electrode made of metal or polycrystalline silicon.

A point in the semiconductor is defined by its distance x with respect to the Si-SiO interface, and y with respect to source. The problem is two-dimensional, i.e. with no field component in the z direction.

The following assumptions are made:

1. In the channel region, the doping is uniform, in the order of 10^{21} to 10^{22} m^{-3}.
2. No generation or recombination effects are present.
3. The channel is long and wide ($\geqslant 20$ µm) with respect to d_{ox} ($\leqslant 0.1$ µm), allowing the "gradual channel assumption": the gradient of the electric field is assumed to be mainly in the x direction (perpendicular to the surface):

$$\left|\frac{\partial E_x}{\partial x}\right| \gg \left|\frac{\partial E_y}{\partial y}\right|$$

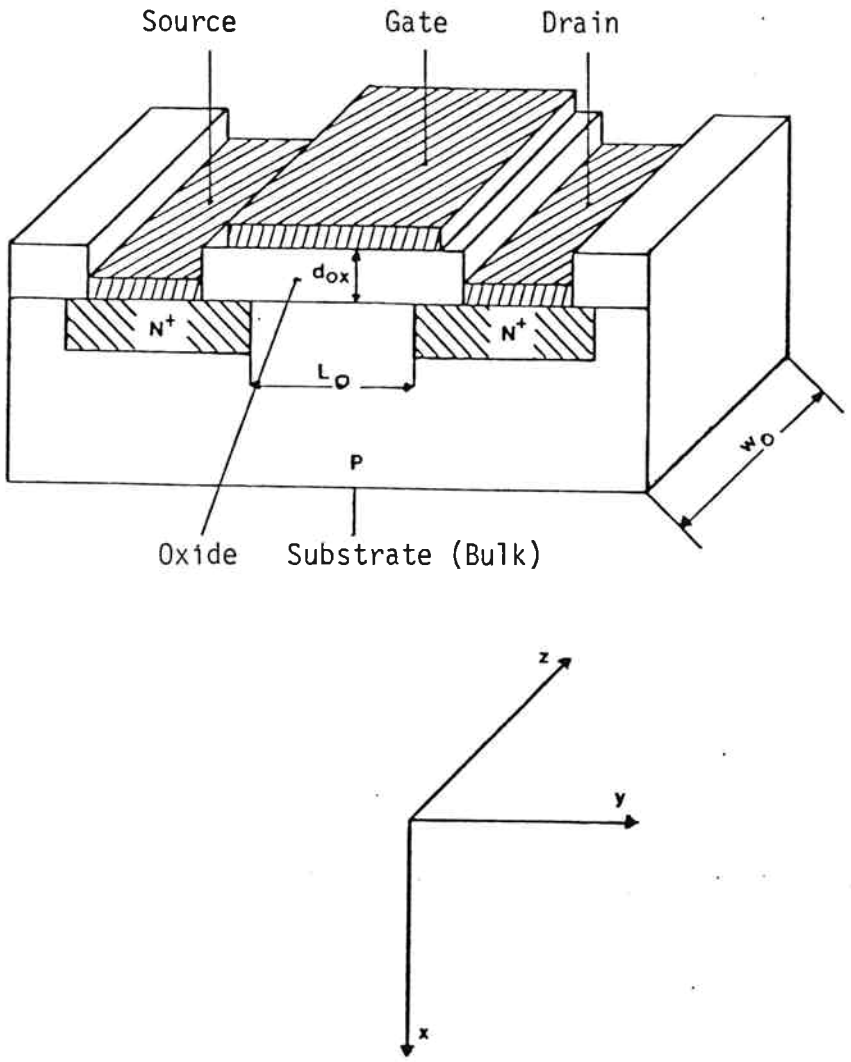

Fig. 1 Schematic cross-section of a MOS transistor.

4. Consequently, the flow of carriers is parallel to the surface, and the total current is constant along the channel, and is produced by a single type of carriers.

5. Mobility is a constant.

6. Absence of mobile charges in the oxide and of fast surface states. A fixed charge in the oxide or at the interface is accepted.

7. Thermodynamic quasi-equilibrium conditions (steady state currents and voltages, uniform temperature).

It is known that some of the assumptions are not accurate in real structures. Corrections will be discussed later.

2.2 Analysis of Pao and Sah

Some important properties of the current can be derived from the analysis of Pao and Sah, which will be discussed here in a slightly different way.

Let us define the source, drain and gate potentials V_S, V_D and V_G with respect to the substrate, and let us normalize all potentials with respect to the thermodynamic potential $U_{TH} = kT/q$: (1)

$$u = \emptyset/U_{TH} \quad \text{or} \quad V/U_{TH} \tag{2}$$

In a n-channel transistor, the p-doped substrate (bulk) has a concentration

$$N_B = n_i \exp u_F \tag{3}$$

The carrier concentrations of the holes (p) and of the electrons (n) are related to the potential u and to the potential difference ξ of the quasi-Fermi levels $\xi = u_n - u_p$:

$$p = N_B \exp(-u) \tag{4}$$

$$n = N_B \exp(u - \xi - 2u_F) \tag{5}$$

Assuming the potential variation is mainly in the vertical direction x, the unidimensional Poisson equation has to be solved:

$$U_{TH} \frac{d^2u}{dx^2} = - \frac{\rho}{\varepsilon_s} = - \frac{q}{\varepsilon_s} (p-n-N_B) \tag{6}$$

A first integration gives the normalized field

$$\frac{du}{dx} = - \frac{1}{L_D} F_1 (u, \xi , u_F) \tag{7}$$

where $L_D = \sqrt{\frac{\varepsilon_s U_{TH}}{2q n_i}}$ is the intrinsic Debye length, and (8)

$$F_1(u, \xi) = \frac{u}{|u|} \sqrt{e^{u- \xi -u_F} + e^{u_F-u} + (u-1)e^{u_F} - (u+e^{- \xi }) e^{-u_F}} \tag{9}$$

is an auxiliary function (normalized total charge density).

The current density at any point x,y is given by

$$J(x,y) = -q D_n n \frac{d\xi}{dy} \tag{10}$$

The total channel current is obtained by integration

$$I = \frac{1}{L_o} \int_o^{L_o} D_n W_o \frac{d\xi}{dy} \int_o^{x_i} q n (x,y) dx dy \tag{11}$$

with W_o and L_o the effective channel width and length.

The second integral represents the inversion charge density. Using (5) and (7), we can write

$$n dx = n \frac{dx}{du} du = \frac{n du}{\frac{du}{dx}} = - \frac{N_B}{L_D} \frac{\exp (u- \xi -2u_F)}{F_1 (u, \xi)} du \tag{12}$$

the limits of integration are converted into the corresponding potentials u_F and u_{surf}, where u_{surf} is the surface potential.

The first integral can be similarly expressed in terms of the potential along the channel, with the boundary conditions u_S at the source and u_D at the drain. The current, normalized by a factor I_T, becomes

$$I = I_T \int_{u_S}^{u_D} F_3 (u'_G, \xi) d\xi \tag{13}$$

with F_3 a function representing the normalized mobile charge:

$$F_3 (u'_G, \xi) = \frac{1}{2} B_2 \int_{u_F}^{u_{surf}} \frac{\exp (u-2u_F - \xi)}{F_2 (u, \xi)} du \tag{14}$$

$$I_T = \mu C_{ox} \frac{W_o}{L_o} U_{TH}^2 \tag{15}$$

$$B_2 = \frac{d_{ox}}{\varepsilon_{ox}} \sqrt{\frac{2q N_B \varepsilon_S}{U_{TH}}} \tag{16}$$

$$F_2 \cong \frac{u}{|u|} [u-1 + \exp(u-2u_F- \xi)]^{1/2} \tag{17}$$

The surface potential is given by the implicit relation relating it to the gate potential u'_G

$$u'_G = u_{surf} + B_2 F_2 (u_{surf}, \xi) \tag{18}$$

where $u'_G = (V_G - V_{FB}) / U_{TH}$ (19)

Finally, the general current-voltage relations are contained in eq. (13) with the boundary condition (18). The first definite integral (13) shows that the current is the difference between two functions $i(V_S)$ and $i(V_D)$. Each of these functions can be defined by choosing its asymptotic value equal to zero when the lower limit tends to a large value:

$$\int_{u_S}^{u_D} = \int_{u_S}^{\infty} - \int_{u_D}^{\infty}$$

We define a function $y(u_C, \xi)$ with $\xi = u_S$ or u_D, in order to represent the two components of the normalized current:

$$y(u'_G, \xi) = \frac{I_x}{I_T} = \int_{\xi}^{\infty} F_3(u'_G, \xi) \, d\xi \tag{20}$$

Now the total current is obtained as a difference of two functions y:

$$I = I_T [y(u'_G, u_S) - y(u'_G, u_D)] \tag{21}$$

This property reminds the decomposition of the current in a forward and a reverse component in bipolar transistors.

An important special case is the grounded source saturation current, for which $u_S = 0$, $u_D = \infty$ and $I_{sat} = I_T \; y(u'_G, 0)$ (22)

This current is a function of u'_G only. Its knowledge is sufficient in many applications.

Numerical integration of (20) has been solved in order to have a basis of comparison for further simplifications. The set of normalized characteristics $y = f(u'_G, \xi + 2u_F)$ is dependent upon a single parameter B_2 (eq. 16). This parameter is represented in fig. 2 as a function of d_{ox} and N. It is generally comprised between 3 and 7. Its value varies with temperature. It is related to the commonly defined bulk factor K:

$$K = B_2 \sqrt{U_{TH}} = \frac{d_{ox}}{\varepsilon_{ox}} \sqrt{2 \varepsilon_S q N_B} \qquad (23)$$

Typical curves of $y = f(\xi)$ are plotted in fig. 3 to 5 on a semilog scale, with u'_G as a parameter, for $B_2 = 3, 5, 7$ and $u_F = 12$.

It appears clearly that, for $I_D < I_T$, these curves represent an exponential dependence of I_D with V_x, with a constant "slope". This is the weak inversion region. For a given value of B_2, the characteristics can be obtained approximately by horizontal translation. For different values of B_2, the curves are still of the same character in weak inversion, but are slightly translated in the vertical direction also, with minor changes in the transition between weak and strong inversion.

2.3 Explicit formulation of the Pao and Sah equations

Many authors tried to find explicit expressions of the Pao and Sah equations. Unfortunately, only approximations are possible. The problem can be decomposed into 4 phases:

1) Weak inversion approximation
2) Limit of the weak inversion region, corresponding to the threshold voltage
3) Strong inversion approximation
4) Analytical expression allowing a continuous interpolation.

2.3.1 Weak inversion approximation

The method used is a mere adaptation of Barron's [72 Ba].

Let us assume $\xi > 0$

$$u_F < u < 2u_F + \xi$$

Then $F_2 \cong \sqrt{u - 1}$ (24)

The surface potential u_{surf} is obtained by solving the equation

$$u'_G = u_{surf} + B_2 \sqrt{u_{surf} - 1} \qquad (25)$$

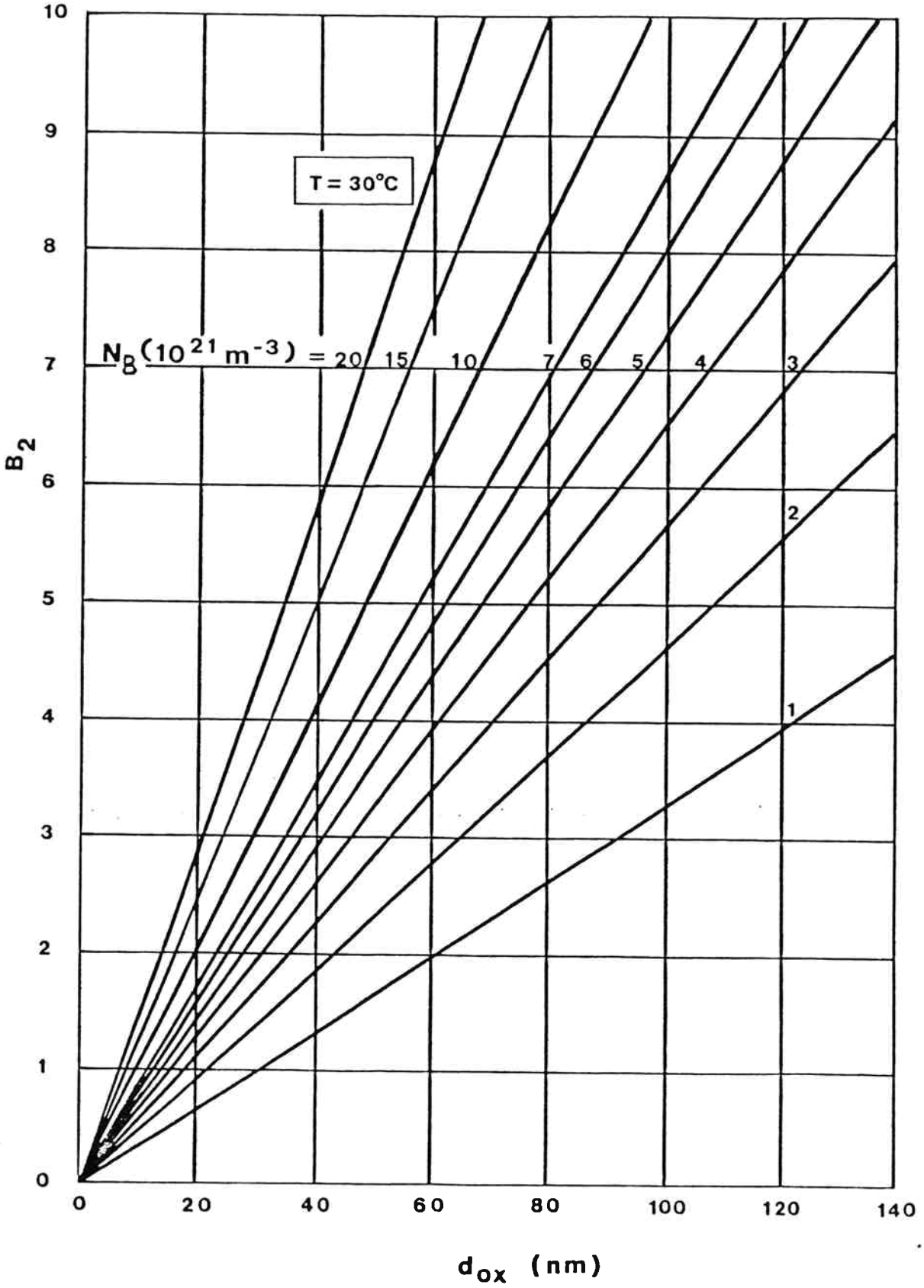

Fig. 2 Body factor $B_2 = K \sqrt{U_{TH}}$ as a function of oxide thickness d_{ox} for several substrate concentrations N_B.

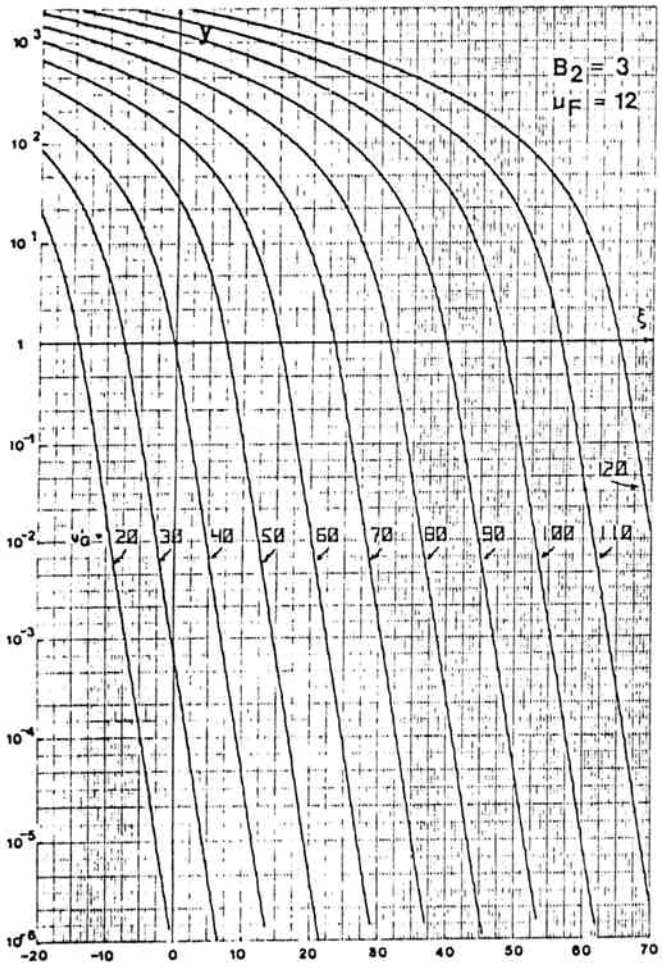

Fig. 3

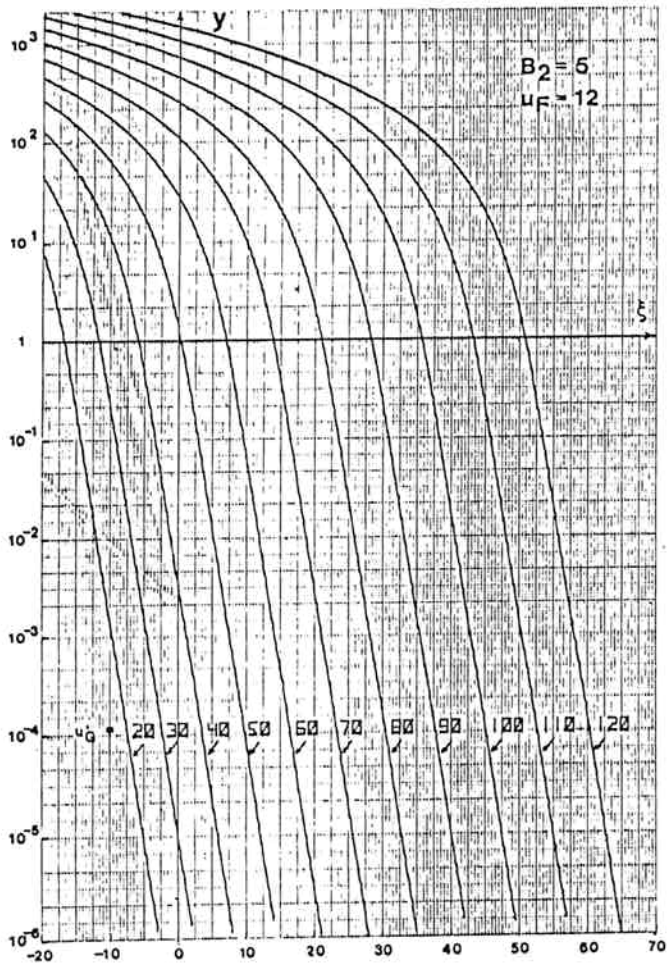

Fig. 4

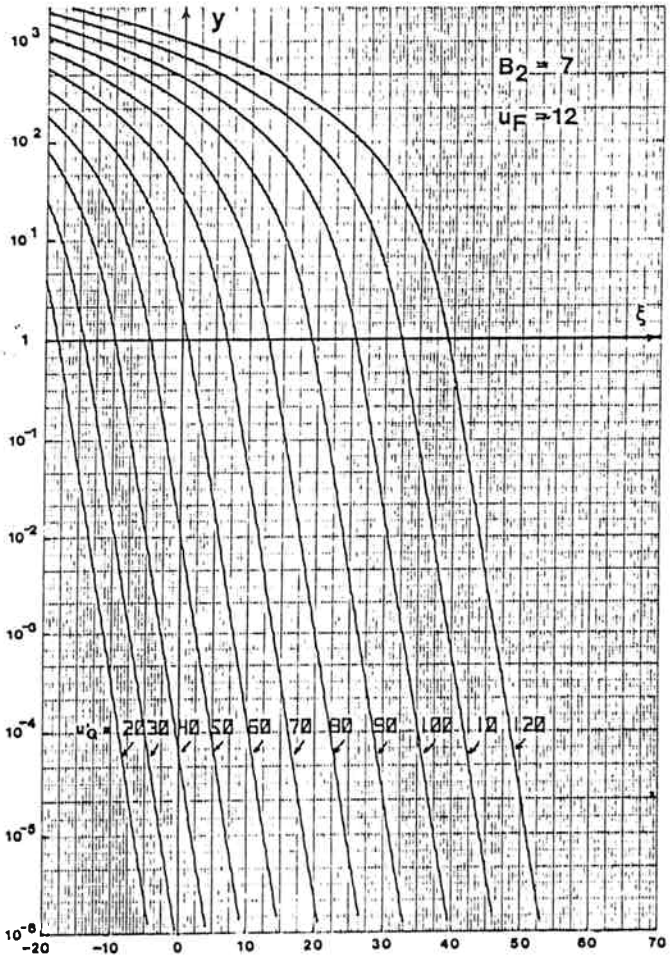

Fig. 5

Fig. 3-5. Normalized saturation current y as a function of the normalized channel potential ξ for 3 values of $B_2 = K\sqrt{U_{TH}}$ and for $u_F = 12$. The same curves are valid for other values of u_F if they are shifted to maintain $2u_F + \xi$ constant.

It has been found useful to define a "control voltage" V_C or its equivalent normalized variable u_C. This voltage will be related to the surface potential u_{surf} in weak inversion but defined by the same mathematical function for the whole range of gate voltages:

$$u_C = u_{surf\ weak\ inv_2} - 2u_F$$

$$u_C = u'_G - 2u_F + \frac{B_2^2}{2}\left(1 - \sqrt{1 + \frac{4u'_G - 4}{B_2^2}}\right) \tag{26}$$

The derivative of this expression is also a meaningful quantity: it will be designed by γ :

$$\gamma = \frac{\partial u_C}{\partial u'_G} = 1 - \frac{1}{\sqrt{1 + \frac{4u'_G - 4}{B_2^2}}} \tag{27}$$

An important property of the surface potential in weak inversion is its independence from the carrier concentration, and from the potential ξ. Consequently, the inversion charge becomes

$$F_3 = \frac{1}{2} B_2 \exp(-2u_F - \xi) \int_{u_F}^{u_{surf}} \frac{\exp u\ du}{\sqrt{u - 1}}$$

Approximate integration is obtained after a series expansion of the denominator around $u = u_{surf}$.

The second integration in (20) is straightforward.

The current function becomes

$$y(u_C, \xi) = \frac{1}{2} B_2 \frac{\exp(u_C - \xi)}{\sqrt{u_C + 2u_F - 2}} \tag{28}$$

It is useful to introduce a "weak inversion function" f_w in accordance with the exponential character of y :

$$y = e^{2f_w} \tag{29}$$

$$\text{with } f_w = \frac{1}{2}\left[u_C - \xi - \frac{1}{2} \ln \frac{4(u_C + 2u_F - 2)}{B_2^2}\right] \tag{30}$$

In order to anticipate some discrepancy between the ideal structure assumed here and a real situation, we replace f_w by a general linear function of u_C and ξ:

$$f_w = a_w u_C - b_w \xi + c_w \tag{31}$$

Practical values of a_w and b_w are close to .5, whereas C_w will be discussed later.

2.3.2 Limit of weak inversion

The physical situation responsible for the transition to strong inversion is a concentration of free carriers comparable or higher than the concentration of fixed charges at the surface of the semiconductor. The threshold condition can be defined precisely by $n_{surf} = N_B$ at the surface; the corresponding surface potential $u_m = u_{surf\ threshold}$ will be, according to (5):

$$\exp (u_m - 2u_F - \xi) = 1 \qquad \text{or simply}$$

$$u_m = 2u_F + \xi \tag{32}$$

This situation corresponds to a normalized threshold potential (from (18))

$$u'_T = u_m + B_2 \sqrt{u_m}$$

$$u'_T = 2u_F + \xi + B_2 \sqrt{2u_F + \xi} \tag{33}$$

and to a finite current, which can be estimated assuming that the weak inversion approximation is still valid:

$$y_m(\xi) = \frac{1}{2} B_2 \frac{1}{\sqrt{u_m - 2}} \cong \frac{B_2}{2\sqrt{2u_F + \xi}} \tag{34}$$

For example, if $B_2 = 5$, $u_F = 12$, $\xi = 0$, then $I_m \cong 0{,}5\ I_T$. Therefore, I_T is a good measure of the threshold current.

The gate threshold voltage V_T is the value of V_G corresponding to $u_C = u_m$:

$$V_T = V_{FB} + 2\emptyset_F + V_x + K\sqrt{2\emptyset_F + V_x} \tag{35}$$

Note that V_G being referred to the bulk, the threshold varies with the channel potential and takes different values from source to drain. The threshold voltage V_{TO} for $V_x = 0$ coincides with the usual formulation.

2.3.3 Strong inversion approximation

Many authors have presented approximate solutions of the strong inversion situation. Sah and Pao [66 Sa] solved their integral equations and proved that the well known expressions of Ihantola and Moll [64 Ih], which take care of the depletion charge, were quite accurate.

We have taken a somewhat different approach in order to be able later to find a complete formulation of the characteristics. Numerical solution of the Pao and Sah integral shows that the whole set of curves can be almost exactly superimposed by horizontal shifting (see fig. 3 to 5). We have introduced a control voltage u_C in weak inversion and we have found that a single function f_w, linear in u_C and ξ, describes the current. Let us try to use these results.

The main difficulty does not arise from the integral (14) but from the implicit relation (18). F_2 (eq. 17) changes in character for $u > u_m$:

$$F_2 \cong e^{\frac{1}{2}(u-u_m)} \sqrt{1 + (u-1)\, e^{(u_m-u)}} \tag{36}$$

The function to be integrated in (17) tends towards an exponential, and it can be shown that an approximate expression of (14) is

$$F_3 \cong B_2 \left[\exp \frac{1}{2}(u_{surf} - 2u_F - \xi) - \sqrt{2u_F + \xi}\right] \tag{37}$$

according to (18), u_{surf} cannot grow to large values because

$$u'_G \cong u_{surf} + B_2\, e^{\frac{1}{2}(u_{surf} - 2u_F - \xi)} \tag{38}$$

An approximate inversion of this expression gives

$$u_{surf} - 2u_F - \xi \cong 2 \ln \left(\frac{u'_G - 2u_F - \xi}{B_2}\right) \tag{39}$$

Consequently

$$F_3 = u'_G - u_{surf} - B_2 \sqrt{2u_F + \xi} \tag{40}$$

$$F_3 \cong u'_G - (2u_F + \xi) - B_2 \sqrt{2u_F + \xi} \tag{41}$$

(39) shows that u_{surf} has to be slightly larger than $2u_F + \xi$ in strong inversion, by an amount slightly dependent upon u'_G. Equation (40) takes care of this dependence, whereas (41) is the usual approximation obtained by neglecting the contribution of the surface potential above $2u_F + \xi$.

The function F_3 (41) represents the channel conductance in strong inversion only, and it has no meaning if it becomes 0 or negative. But the condition $F_3 = 0$ can be used to define the "extrapolated threshold voltage" V_T.

Fortunately, it comes to the same expression as (33), a proof that at least the first order terms have been taken care off. The condition $F_3 = 0$ can also be used to investigate the drain saturation voltage $\xi = u_{Dsat}$.

Solving (41) gives

$$u_{Dsat} = u'_G - 2u_F + \frac{B_2^2}{2} \left(1 - \sqrt{1 + \frac{4u'_G}{B_2^2}}\right) \tag{42}$$

this expression is very close to the definition of u_C (26); the only difference is in the expression under the square root; but it is minor for practical values of u'_G (> 50).

Both situations reflect actually the limit of weak inversion, either at the source or at the drain. It is therefore advantageous to identify the control voltage u_C with the drain saturation voltage u_{Dsat} (42). Let us introduce u_C in (41):

$$F_3 = u_C - \xi + B_2 \left[\sqrt{u_C + 2u_F} - \sqrt{\xi + 2u_F}\right] \tag{43}$$

Let us express this function by a Taylor series in $u_C - \xi$. The deviation from a linear law can be neglected, so that F_3 becomes

$$F_3 = (u_C - \xi) \left[1 + \frac{B_2}{2\sqrt{u_C + 2u_F}}\right] \tag{44}$$

The current function y is obtained easily by integration of (44):

$$y(u_C, \xi) = \frac{1}{2} \left(1 + \frac{B_2}{2\sqrt{u_C + 2u_F}}\right) (u_C - \xi)^2 \tag{45}$$

This quadratic expression should be fairly accurate up to moderate current levels. To take other effects into account, we can introduce a strong inversion function f_h such that

$$y = f_h^2 \tag{46}$$

and keep the assumption that f_h be a linear function of u_C and ξ :

$$f_h = a_h (u_C - u_h) - b_h \xi \tag{47}$$

Comparing the expressions (45) and (46) with the numerical results as well as with numerous experiments, it has been found that (47) is quite a good approximation if we take

$$a_h = b_h \cong 0.68 + 0.02\, B_2 \tag{48}$$

$$u_h = 1 \tag{49}$$

Accordingly, more precise definitions of the extrapolated threshold V_{TO} and of the drain saturation voltage V_{Dsat} can be deduced from (47):

$$V_{TO} = V_{FB} + U_{TH} [2u_F + 1 + B_2 \sqrt{2u_F}] \tag{50}$$

$$V_{Dsat} = U_{TH} (u_C - 1) \tag{51}$$

If parameters have to be extracted from experimental data, V_{TO} can be measured precisely, but V_{FB} is not well known. V_{FB} can be eliminated, so that u'_G and u_C are directly related to measurable quantities:

$$u'_G = \frac{V_G - V_{TO}}{U_{TH}} + 2u_F + 1 + B_2 \sqrt{2u_F} \tag{52}$$

$$u_C = \frac{V_G - V_{TO}}{U_{TH}} + 1 + B_2 \left[B_3 - \sqrt{\frac{V_G - V_{TO}}{U_{TH}} + B_3^2} \right] \tag{53}$$

$$\text{with } B_3 = \frac{1}{2} B_2 + \sqrt{2u_F} . \tag{54}$$

2.3.4 Analytical formulation for the whole range of current and voltage values

Pao and Sah's formulation is continuously valid in all biasing regions, but it requires numerical calculations.

Brews [78 Br] succeeded, by using the charge-sheet concept, to obtain an explicit expression of the current as a function of the gate voltage and of the surface potentials at the source ($u_{\beta S}$) and at the drain $u_{\beta D}$. In our notation, the normalized current becomes

$$\frac{I}{I_T} = (u'_G + 1)(u_{\beta S} - u_{\beta D}) - \frac{1}{2}(u_{\beta S}^2 - u_{\beta D}^2) - B_2 \left\{ \frac{2}{3}(u_{\beta S} - 1)^{3/2} - \frac{2}{3}(u_{\beta D} - 1)^{3/2} - (u_{\beta S} - 1)^{1/2} + (u_{\beta D} - 1)^{1/2} \right\} \tag{55}$$

For given gate, source and drain voltages, the surface potentials have still to be computed in an iterative way from (18). Other authors came essentially to the same result [79 Wi, 83 Pi, 83 Gu]. This expression is useful in strong inversion for which the surface potential near the source can be computed from (39), and the surface potential near the drain from (39) below saturation or from (25) in saturation. In weak inversion, some numerical problems can arise from the fact that the current results as a small difference of large numbers.

Several authors use two different explicit formulations, one for weak inversion and another for strong inversion, fitting them for a continuous transition around the threshold voltage [72 Sw, 75 Sw, 79 Ta]. Another approach is to add up the usual strong inversion current with a subthreshold current; this subthreshold current is calculated with the usual weak inversion formula but limiting its value at the approach of the threshold [82 Ya, 82 An].

After the observation that the weak and strong inversion conditions can be described conveniently by means of the control voltage u_C and two linear functions f_w and f_h, we arrived at the following formula, which provides a continuous transition between the two limiting cases:

$$y\,(u_C, \xi) = \frac{1}{\eta^2} \ln^2 \left[1 + \eta\, e^{f_w} + e^{\eta f_h}\right] \qquad (56)$$

This expression tends to the exponential function of f_w for $0 > f_w > f_h$ in accordance with (29) and to a quadratic function of f_h for $0 < f_w < f_h$ in accordance with (46).

The numerical factor η is close to 1, but it allows for a better fitting of the interpolation and to specify the current at an intermediate gate voltage near threshold.

As a proof of the adequacy of the approach taken, the following verification has been made: assuming a given set of parameters B_2, u_F, u'_G, ξ, the functions u_C (26) and f_w (28) were first computed. From the numerical solution of (20), y is also known. As a last step, the ideal values of f_h are computed by inversion of (56). Results are shown in fig. 6 and 7, proving that f_h can be accurately fitted with a linear function in ξ (fig. 6) and in u_C (fig. 7) as long as it is positive. The bending of f_h curves for negative values indicates that the interpolation will be of limited accuracy just below threshold.

2.3.5 Summary of the basic philosophy of the model

Five important steps lead to the model. They are illustrated in fig. 8:

a) Definition of a control voltage V_C, related to $V_G - V_T$ by a slightly non-linear function, with the body factor K as parameter ; V_C is equal to the surface potential in weak inversion.

b) Expression of the current by a difference of two particular values of the same function $y\,(V_C, V_x)$ with the respective values $V_x = V_S$ and $V_x = V_D$.

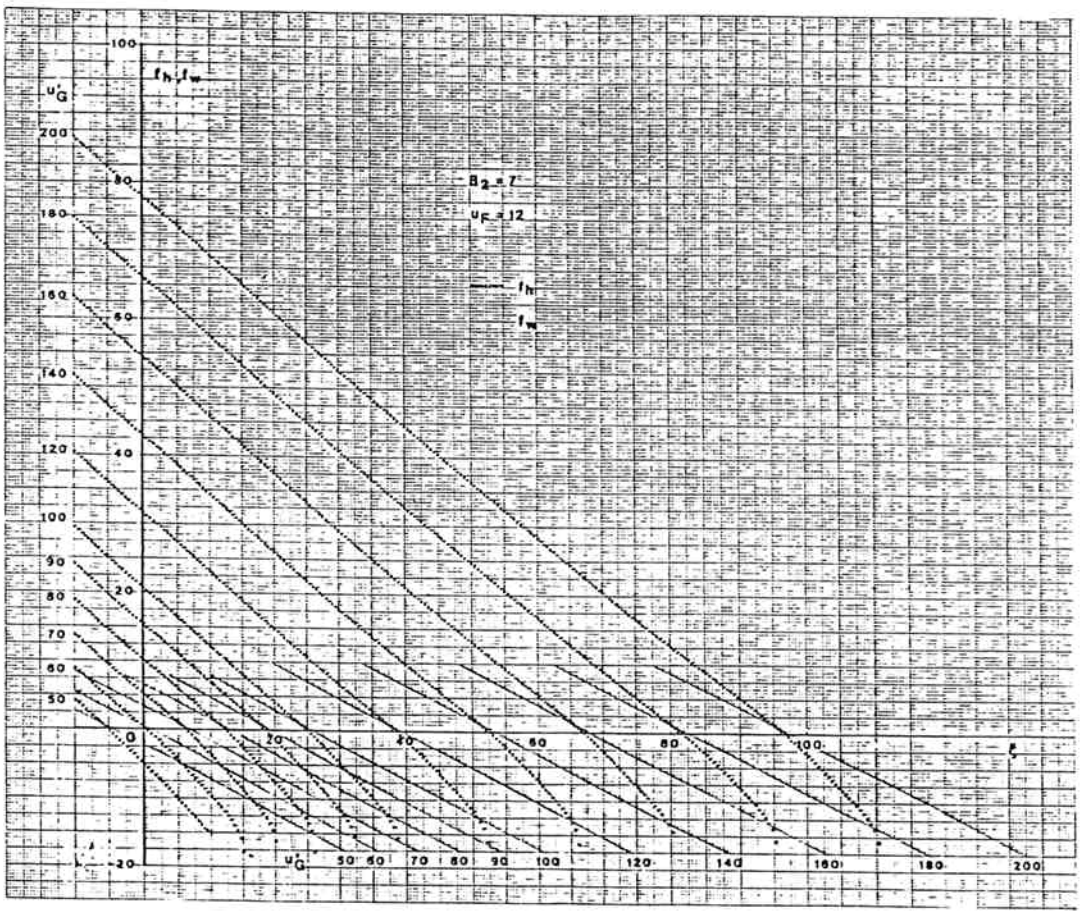

Fig. 6 Example of ideal values of f_h and f_w as functions of ξ.

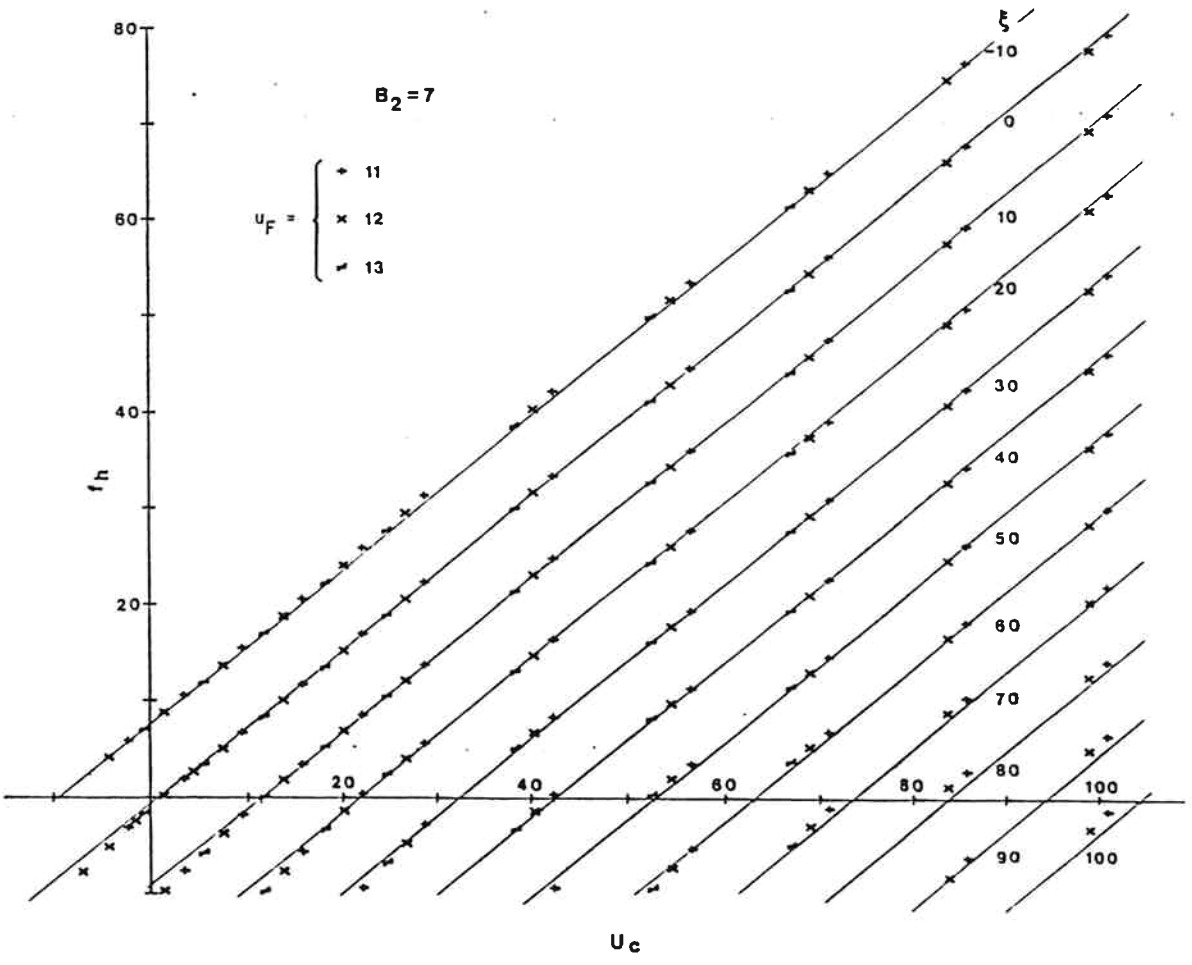

Fig. 7 Example of ideal values of f_h as functions of u_C.

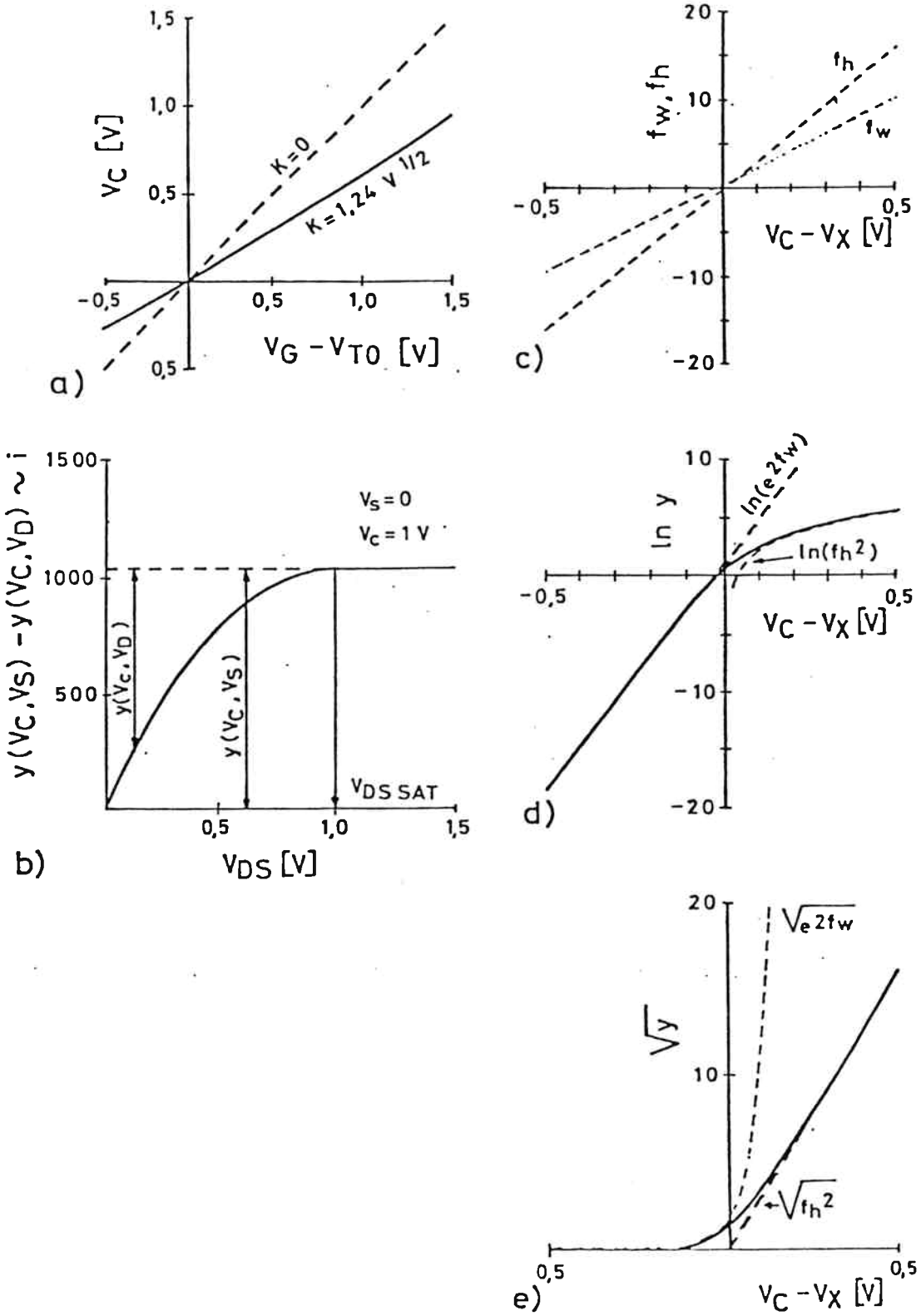

Fig. 8 Illustration of the main steps for an explicit formulation of the ideal MOSFET characteristics:

a) Definition of control voltage V_C

b) Drain current obtained by superposition of two functions $y(V_C,V_X)$ for $V_X = V_S$ and $V_X = V_D$

c) Definition of two linear functions f_w and f_h in V_C and V_X

d) y has the weak inversion asymptote $\exp(2f_w)$

e) y has the strong inversion asymptote f_h^2 .

c) Definition of two auxiliary functions f_w and f_h, linear in V_C and V_x and approximately proportional to $V_C - V_x$.

d) Weak inversion described by $f_w \sim \exp (V_C - V_x)$.

e) Strong inversion described by $f_h \sim (V_C - V_x)^2$.

f) Interpolation formula insuring a continuous mathematical expression in the whole range of voltages and current.

3. Improvements of the long channel model

The long channel model is quite satisfactory for low and medium current density and for channel lengths down to about 20 µm. Nevertheless, a discussion of its limitations and possible extensions is necessary in order to make it useful as a basic CAD model.

Following extensions will be considered:

- Variable mobility
- Influence of channel length
- Weak inversion effects, including surface states and non-uniform doping
- Short-channel effects.

These extensions are more or less straightforward in view of the number of publications covering detailed discussions of these effects. No attempt will be made to give an historical account of them.

3.1 Variable mobility

Mobility is a difficult parameter to characterize, as it is supposed to represent the fairly complicated scattering phenomena which limit the flow of carriers in an MOS transistor.

Mobility is a function of doping and of temperature. It is further a function of the electric field, with different contributions of the transversal field (no net current flow) and of the longitudinal field (in the direction of current, including velocity saturation effects).

Attempts have been made to take into account the local field dependence of mobility before integration [72 ME, 73 Ro]. But the resulting expressions are quite complicated. The heuristic approach consists simply to correct the mobility in the I_T coefficient (16). The most important effect is due to the transversal effect and is related to V_C (or u_C); a second order effect is observed in short channel transistors, and is related to V_D. Both effects are modellized in the following expression:

$$\frac{\mu}{\mu_o} = \frac{1}{1 + \Theta V_C + \frac{V_D^* - V_S}{E_C L_o}} \qquad (57)$$

Here V_D^* is an expression representing either the drain voltage or the saturation voltage $V_{Dsat} = V_C$ as asymptotic values:

$V_D^* = V_D$ if $V_D < V_{Dsat} - 0{,}1$ V

$V_D^* = V_{Dsat} = V_C$ if $V_D > V_{Dsat} + 0{,}3$ V

The interpolation function (52) defined in our model is taken once more in order to provide a continuous transition between these values; V_D^* is computed as follows:

$$V_D^* = V_C - U_{TH} \sqrt{y(u_C, u_D)} / b_h \tag{58}$$

3.2 Influence of channel length

The gradual channel approximation is no more valid if $V_D > V_{Dsat}$. In a short region near the drain, the vertical field vanishes and then takes the opposite direction, and the horizontal field becomes large. Many authors have analyzed this situation. For channel lengths larger than about 50 d_{ox}, the channel is decomposed (fig. 9) into a main region of effective length $L_o - \ell_{dep}$ for which the Pao and Sah approximation is valid, and a short region of length ℓ_{dep} near the drain, in which the carriers travel very fast.

The current is given by

$$I = I_{sat} \frac{L_o}{L_o - \ell_{dep}} \tag{59}$$

In the drain region, the potential varies from an initial value V_p at the interface to the final value V_D, whereas the field varies from E_p to E_D. Under the assumption that $V_p \cong V_{Dsat}$ and $E_p \cong 0$, the one-dimensional solution of the Poisson equation gives

$$\ell_{dep} \cong \sqrt{\frac{2 \varepsilon_S (V_D - V_{Dsat})}{|\rho|}} \tag{60}$$

A mean value of the charge density is

$$\rho = -q N_B + \frac{I}{W_o x_{CH} v} \tag{61}$$

where $\frac{I}{W_o x_{CH}}$ is the mean current density in a channel of depth x_{CH}, and v is the speed of the free carriers, assumed close to its upper limit. x_{CH} is likely to be of the order of the junction depth x_j, but is not precisely known.

The expression of ℓ_{dep} is not valid for $V_D \leqslant V_{Dsat}$. It is transformed into an expression of general validity if V_{Dsat} is replaced by V_D^* (eq. 58).

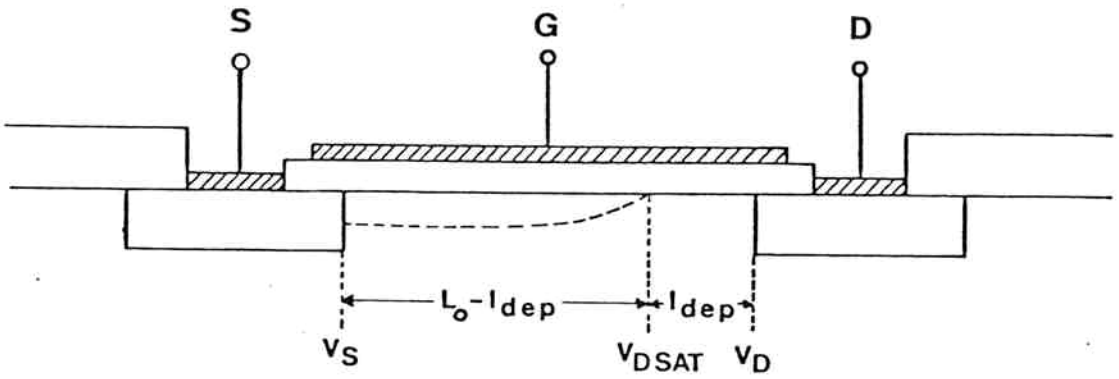

Fig. 9 Usual decomposition of the channel into an inverted region extending from source to $L_o - \ell_{dep}$ and a depleted region of length ℓ_{dep} up to the drain.

Further, two coefficients λ_1 and λ_2 are introduced to fit the formula with experiments. λ_1 takes into account the not well defined parameters describing the mobile charge (especially x_{CH}) and λ_2 stays for deviations from the one sided abrupt vertical junction formula. The result is:

$$\ell_{dep} = \frac{\lambda_2}{b_h}\left[\frac{2\,\varepsilon_S}{q\,N_B}\quad\frac{V_D - V_D^*}{1+\lambda_1 y(u_C,u_S)}\right]^{1/2} \tag{62}$$

3.3 Corrected expression of the strong inversion current

Taking both the channel length modulation and the mobility variation into account, the corrected current becomes in strong inversion

$$I = \frac{BU_{TH}^2}{2b_h^2}\left[y\,(V_C, V_S) - y\,(V_C, V_D)\right] \tag{63}$$

$$\text{with}\quad B = \frac{B_o}{\left[1 + \Theta V_C + \frac{V_D^* - V_S}{E_C\,L_o}\right]\left[1 - \frac{\ell_{dep}}{L_o}\right]} \tag{64}$$

$$\text{and}\quad B_o = 2b_h^2\;\mu_o\,C_{ox}\;\frac{W_o}{L_o} \tag{65}$$

W_o and L_o are effective dimensions at low field. They should be corrected, if layout dimensions are given, by corrections involving lateral diffusion and other effects taking place during fabrication:

$$W_o = W + \Delta W \tag{66}$$

$$L_o = L - \Delta L$$

3.4 Weak inversion effects

In the ideal Pao and Sah situation, the weak inversion current is explicitely known (eq. 28). In replacing this accurate expression by a pure exponential function, 3 parameters a_w, b_w and C_w have been introduced. Their values are known in the ideal situation, but they can also be considered as free parameters able to describe some new physical effects, as long as the general character of the current behaviour is not altered.

Muls et al [78 Mu] analyzed in depth the influence of many physical effects on the weak inversion characteristics of MOSFETs.

3.4.1 Fast surface states

The effect of fast surface states is equivalent to a capacitance C_{ss} which absorbs some of the charges flowing to the channel. Assuming an uniform distribution around the middle of the forbiden gap, the relation between u'_G and u_{surf} will be modified as follows [72 Sw]

$$u'_G = u_{surf} + B_2 \sqrt{u_{surf} - 1} + \frac{C_{ss}}{C_{ox}} (u_{surf} - \xi) \tag{67}$$

For a given u'_G, this expression means that u_{surf} varies slightly with ξ in weak inversion. The parameters a_w and b_w are affected as follows:

$$2a_w = \frac{\partial \ln y}{\partial u_{surf}}\bigg|_{\xi = ct} = 1 - \frac{1}{2u_{surf} - 4} \tag{68}$$

$$2b_w = \frac{\partial \ln y}{\partial \xi}\bigg|_{u'_G = ct} = 1 - \frac{C_{ss}}{C_{ox}} \gamma \left(1 - \frac{1}{2u_{surf} - 4}\right) \tag{69}$$

a_w should not be affected by surface states, but b_w should be slightly less than 1/2.

Swanson et al [72 Sw] consider two parameters m and n related to the ratio of capacitances C_D (depletion), C_{ox} and C_{ss} in weak inversion.

$$m = \frac{\partial V_G}{\partial V_S}\bigg|_{I = ct} = 1 + C_D/C_{ox} \tag{70}$$

$$n = \frac{1}{U_{TH} \frac{\partial \ln I}{\partial V_G}\Big|_{V_S = ct}} = 1 + (C_D + C_{ss})/C_{ox} \tag{71}$$

Our weak inversion parameters are related to m and n in the following way:

$$b_w = \frac{1}{2} \frac{m}{n} \tag{72}$$

$$a_w = \frac{1}{2 \gamma n} \tag{73}$$

As $\gamma = \frac{\partial V_C}{\partial V_G}$ is a slowly varying function of V_G, m and n are dependent upon V_G whereas a_w and b_w are constant. If no other effect is present, especially the substrate is homogeneous, the density of surface states can be immediately deduced from the difference n-m.

3.4.2 Non-uniform doping

Non-uniform doping is always present in MOS structures due to redistribution effects during oxide growth and often due to the use of ion implantation in the channel.

According to the lucid discussion of Brews [81 Br], subthreshold characteristics depend only upon the depleted portion of the implanted dose, D_I ions per unit area, and upon the centroid of this portion, at a distance x_C of the surface (see fig.10). The threshold shift with respect to an unimplanted substrate is approximately:

$$\Delta V_T = B_2\, U_{TH} \left\{ \frac{D_I}{\sqrt{2}\, N_B L_B} + \left(u_{surf} - \frac{D_I\, x_C}{N_B\, L_B^2} - 1\right)^{1/2} - (u_{surf}-1)^{1/2} \right\} \qquad (74)$$

If the implanted dose is contained completely in the depletion region, D_I and x_C are constants describing the implanted profile. Otherwise both D_I and x_C will be function of u_{surf}.

A second effect of implantation is to modify the slope $\frac{\partial \ln I}{\partial u'_G}$ which is identified with $2a_w \gamma$ in our model. Shannon [71 Sh] has devised a method to extract the profile from d.c. measurements in weak inversion according to the relation:

$$\frac{\partial}{\partial V_S} \left(1 - \frac{\partial V_G}{\partial V_S}\right)^{-2} = \frac{-2\, C_{ox}^2}{q\, \varepsilon_S N_B(x)} \qquad (75)$$

where the derivatives indicate a constant current level. Relating this expression with the CEMOS weak inversion parameters, we find:

$$\frac{\partial}{\partial V_S} \left(1 - \frac{b_w}{\gamma\, a_w}\right)^{-2} = \frac{2\, C_{ox}^2}{q\, \varepsilon_S\, N_B(x)} \qquad (76)$$

This relation implies generally that the ratio $\frac{b_w}{a_w}$ will be dependent upon the doping profile, and therefore upon V_S in a constant current measurement. This fact puts a limitation to the validity of the present model, because the simulated characteristics will fit with experimental data in a limited range of source voltages.

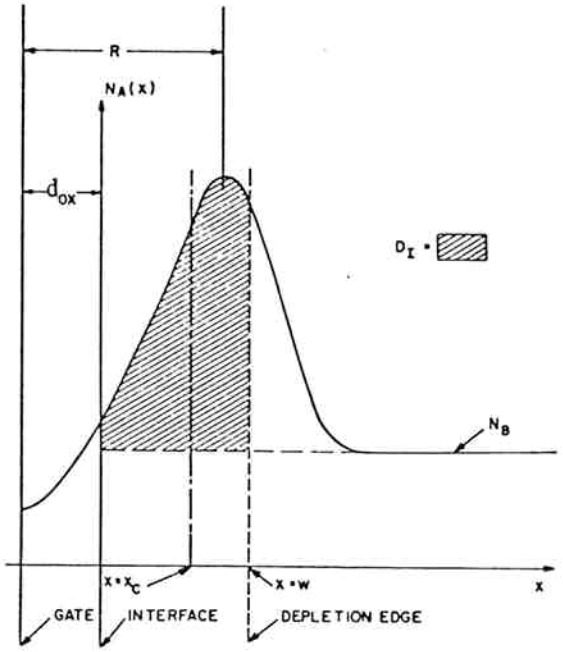

Fig. 10 Schematic of doping profile of an implanted device. The shaded portion of the profile is the portion in the depletion region, D_I. The centrodoid of the shaded region is labelled $x = x_C$ (From Brews [81 Br]).

3.4.3 Other weak inversion effects

According to Muls et al [78 Mu], other effects expected in weak inversion are potential fluctuations along the channel and a possible reduction in mobility. These effects have not been explicitely included in the model, but they are likely to modify the parameters a_w, b_w and C_w.

The absolute current level in weak inversion has to be adjusted after parameter extraction in strong inversion. It has been found of practical advantage to replace the additive constant C_w in the expression (31) by a multiplicative constant K_w associated with the weak inversion term. This represents a simple modification in the final formulation given in the appendix 1.

3.5 Short channel effects

Medium and long channel devices are characterized by a set of parameters which can be specified with acceptable tolerances for a well established technology. As channel length is reduced ($L_o \lesssim 10$ µm) departures occur first in parameter values, then for very short channels ($L_o \lesssim 2.5$ µm) in device behaviour. The limits separating medium, short and very short channel lengths are of course technology dependent; for example with a technology specially designed to make very short transistors [82 Fi], very short channel behaviour is observed for $L_o = 0.14$ µm but not for $L_o = 0.19$ µm.

For short channels the following effects should be considered:

- Reduced values for K and V_{TO}
- Modified values for a_w, b_w, K_w and η
- Velocity saturation
- Series resistances .

Short channel as well as narrow channel effects on K and V_{TO} are explained by the charge-sharing concept. The two-dimensional potential modifies the amount of depletion charge which is controlled by the gate compared to the one-dimensional long channel theory. Much literature was dedicated to this subject; both for two-dimensional simulations and for geometric approximations, it has been found that the body-effect parameter K should be expressed by its theoretical (one-dimensional) value multiplied with a charge sharing factor F

$$K_{eff} = F\,K \qquad (77)$$

This new K_{eff} should be considered in calculating the threshold voltage from the equation (35).

The charge-sharing factor F can be obtained from structure and process parameters by simple geometric considerations [74 Ya, 77 Fu, 78 Ta, 81 Br]. They are generally bias dependent and not very precise [82 Ra, 83 Si], except when well fitted.

For not very short devices we preferred a simpler approach: K_{eff} and V_{TO} are extracted in the same way as for longer devices and used as constant parameters in the model equations. The precision of the simulation is not as good as for longer devices, bit still acceptable both in weak and in strong inversion. The weak inversion parameters a_w, b_w and K_w, extracted in the usual way, have reduced values; their fitting action compensates for the substrate bias effect on the charge-sharing factor. The interpolation parameter η increases as a result of a reduced K_w.

In strong inversion, an increased mobility degradation which depends also on substrate and drain bias is observed for short transistors. Such a behaviour is explained by velocity saturation and series resistances. The velocity saturation effects are noticeable in n-channel MOSFETs only; they are expressed with the critical field E_C (eq. 57) whose values vary with the channel length, as already reported [80 Kl], and with the temperature (slight decrease). Contrary to other models [79 Ho, 80 Vl, etc], no correction of V_{Dsat} is necessary for short channels. Series resistances are estimated on special test figures or from measurements at small V_{DS} and high V_{GS} of several transistors with different lengths but same width and source and drain geometries (hopefully same series resistances). These measurements yield also ΔL [80 Ch].

Typical very short channel behaviour ($L_o \simeq 2.2$ µm) is shown in fig. 11. The big drain voltage dependence of the weak inversion current (almost exponential) and the reduced body effect are explained by a two-dimensional punch-through like drain induced barrier lowering effect [74 Tr, 79 Tr, 79 Ki, 80 Li]. Similar characteristics (fig. 12) are obtained in a two-dimensional simulation with the PTIMOS program (appendix III) for a device corresponding approximately to the measured device.

It is interesting to point out that the current increase with the drain voltage slows down when the threshold voltage (0.52 V for this device at

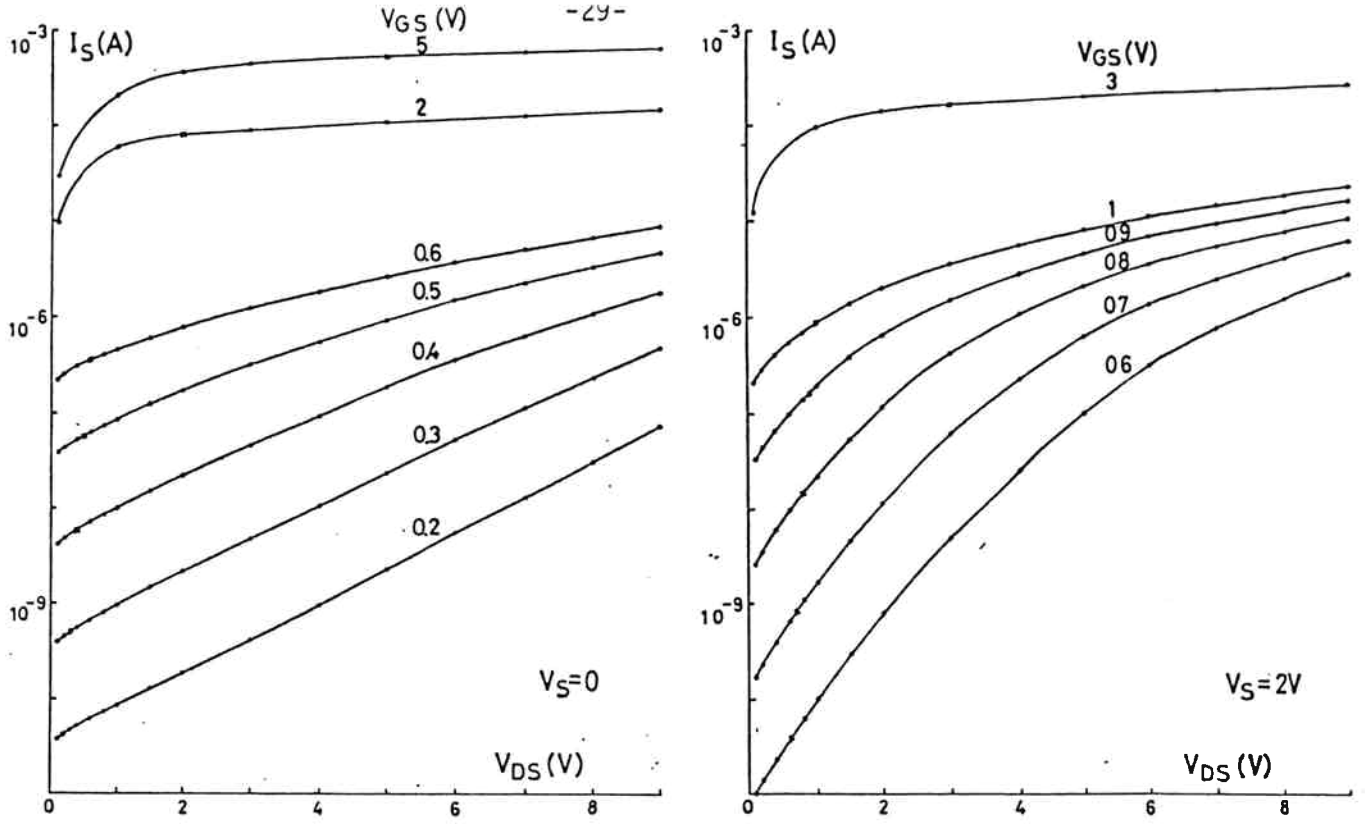

Fig. 11 Measured source current versus drain voltage characteristics at two substrate biases with gate voltage ranging from weak to strong inversion for a very short p-channel transistor (L_o = 2.2 µm, W_o = 20 µm, V_{TO} = 0.52 V).

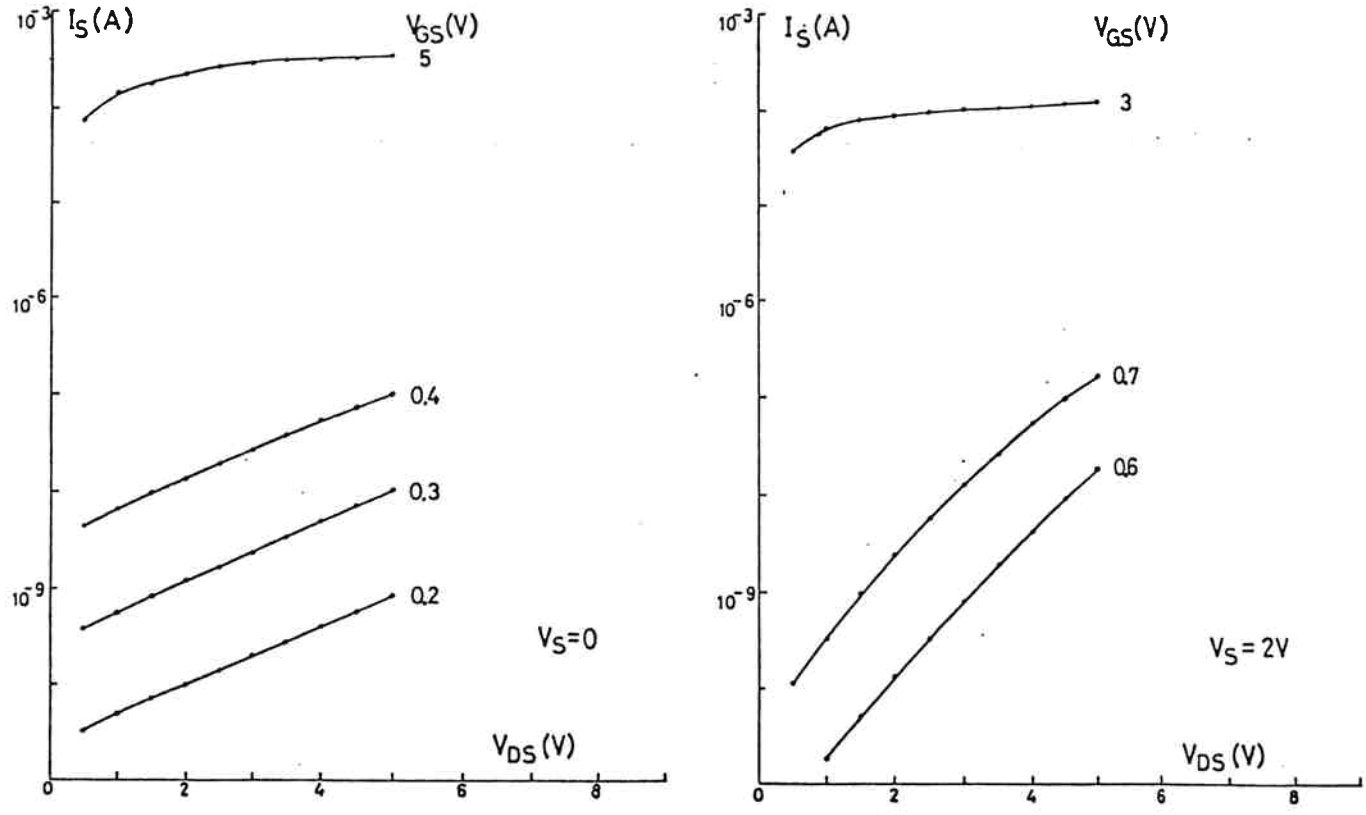

Fig. 12 The same characteristics as in fig. 11 calculated with the PTIMOS two-dimensional program for a similar transistor (constant doping 1.85 x 10^{15} cm^{-3}, V_{FB} = -0.6 V, PTIMOS default mobility model with μ_o = 300 cm^2/Vs).

V_S = 0) and the corresponding current level are approached. Finally, in strong inversion, the saturation current is very well described by the model equation with the same parameter values ($\lambda_1 L_o, \lambda_2$) as for longer transistors.

Weak inversion characteristics are compared for this very short transistor with a typical long transistor in fig. 13. The very short device shows reduced body effect and threshold voltage, and both are decreasing for increasing drain voltage, results corresponding to expected charge-sharing factor variations. But the slopes for the V_S = 0 characteristics are almost identical; steeper characteristics were expected for a reduced body factor coefficient (increased γ, reduced n). For an even shorter transistor (L_o = 1.6 µm) a small decrease in the slope was observed, as predicted by two-dimensional computer calculations [79 Ko] and explained by reduced gate voltage control on the barrier height which determines the current in punch-through situation (the potential distribution presents a saddle point which is further away from the surface).

How can the drain induced barrier lowering be modelled ? Taylor [78 Ta] claims that a voltage dependent charge-sharing factor is able to model all effects, but its current expression (29) predicts a reduced n which does not correspond to experiment nor to two-dimensional simulation. Yang and Chatterjee [82 Ya] simplify F to a function of drain voltage only, which happens to fit quite well with our measurements of the K_{eff} dependence on drain voltage, but their F should be corrected to include the important effect present at small drain voltages. Another approach [77 Tr, 80 Kl] takes into account a linear reduction in threshold voltage with drain voltage, eventually including a charge-sharing factor dependent on body bias only [80 Vl]. We found indeed a linear variation of the threshold voltage (measured at constant current) with drain voltage, but the slope changes with V_S (fig. 14). A better modelling of observed very short channel threshold variation is obtained [82 Ra] with a more elaborate expression.

No further effort was made to incorporate very short channel effects in our model. In fact they do not occur for the shortest transistor used normally in our present technology. The extreme example given before [82 Fi] shows that with a special technology even a 0.19 µm long transistor is not very short ! Furthermore, very short channel effects occur together with extreme dispersion of the characteristics, as in Taylor's [78 Ta] fig. 9.

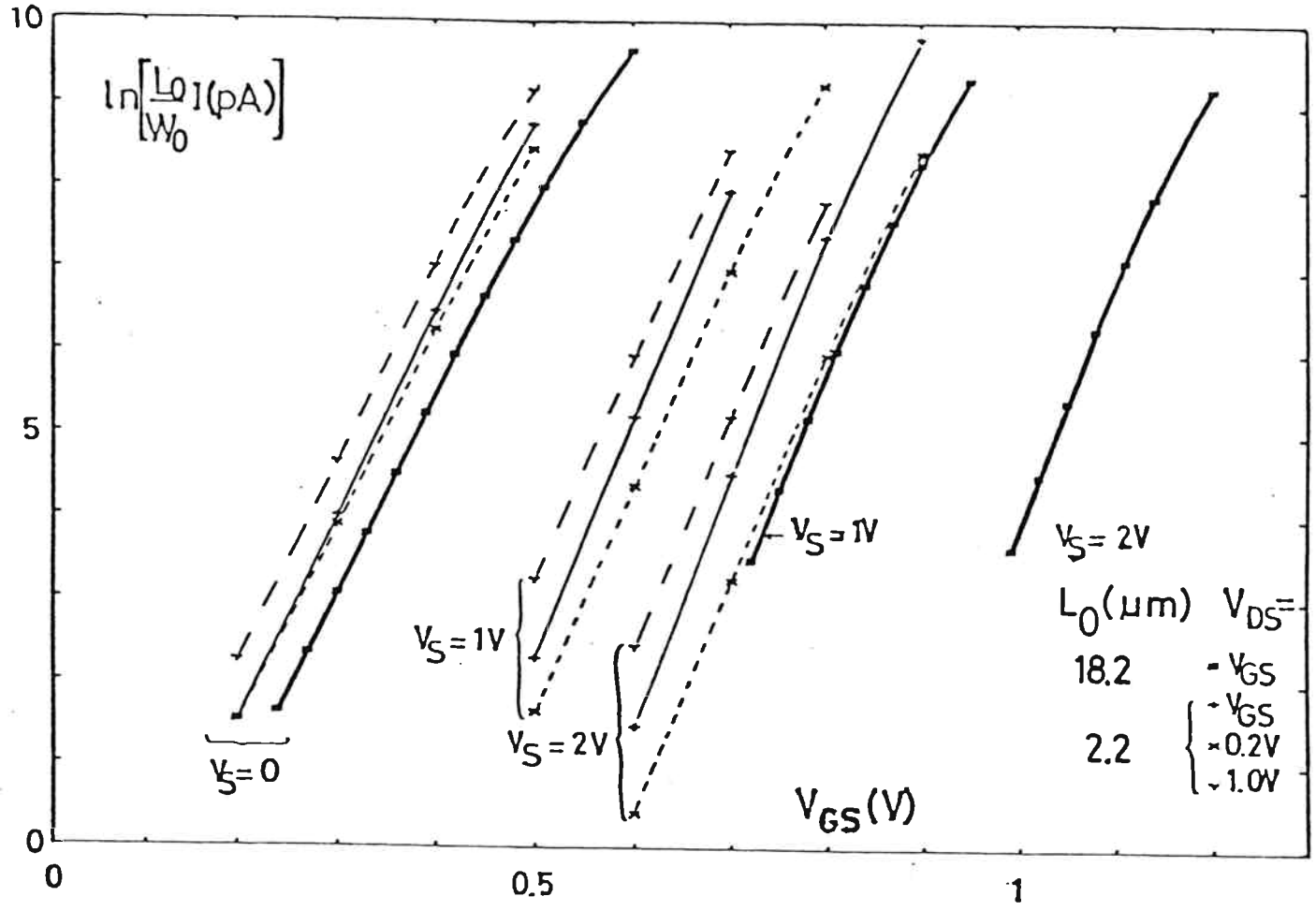

Fig. 13 Subthreshold current versus gate voltage for the short transistor from fig. 11 compared to the same characteristics represented in thick lines for a typical long transistor.

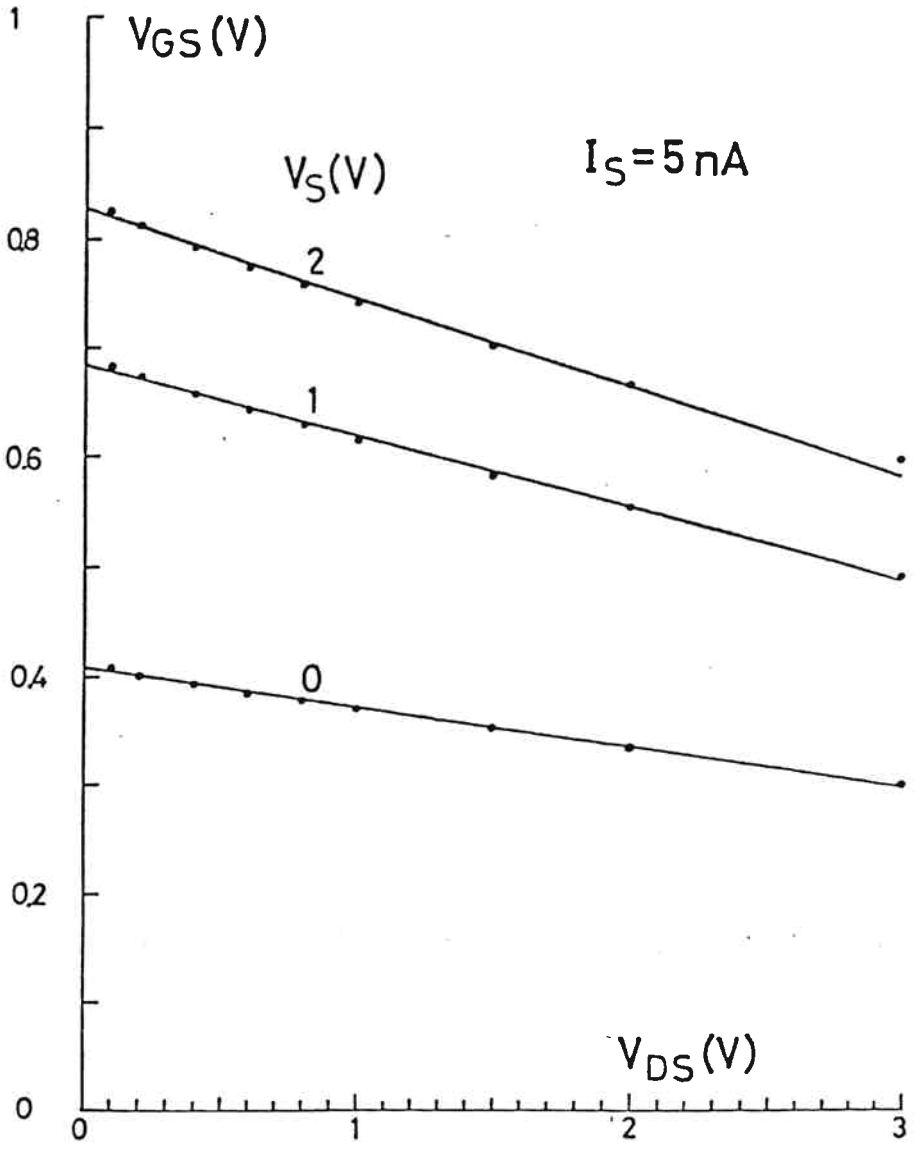

Fig. 14 Measured threshold voltage versus drain bias at several substrate biases for the same transistor as in fig. 11.

Device designers will use two-dimensional simulation to find out how to eliminate very short channel situations; this problem is not very important for circuit simulation.

3.5 Summary of the CEMOS model - Explicit formulation of the current and of the conductance

The complete model has received the name CEMOS (Computer Evaluation of MOS transistors). A summary is given in the appendix I (CEH Catalogue 2.2.1/1.3). Explicit voltages and conventional formulation are used. This model is incorporated in CAD programs (DOMOS, SPICE). From the equations, explicit expressions of the derivatives can be extracted.

Besides the capability of the model to describe the weak to strong inversion transition by means of a continuous set of equations, the simple relations corresponding to the limiting cases are also useful. They are summarized on the second page, together with the derivatives (conductances).

4. Parameter extraction and comparison with measured MOSFETs

Some scientists are of the opinion that any curve fitting is a sign of the weakness of a model. In the present case, we have adopted the opposite attitude, and tried to fit every parameter of the model with a definite set of experimental points for a number of transistors and to check afterwards the following points:

1) Examine other experimental points of the measured transistors and how much do they deviate from the simulated values. As we have to deal with a current able to vary by some 9 orders of magnitude and which depends on 3 voltages, this is already a severe proof.

2) How do the extracted parameters agree with expected values obtained by different means, for example by capacitance measurements ?

3) How close are the parameters extracted from different MOSFETs of different dimensions, possibly with different gate oxide thicknesses ?

4) Is the temperature dependence of the parameters in accordance with the expected physical situation ?

The procedure of parameter extraction is the result of a number of trials along these four directions. The order in which the parameters are determined is given in Table 1 together with the domains in which the corresponding points (numbered from 1 to 12) are located.

TABLE 1. CEMOS parameter extraction

Known parameters: T (U_{TH}, n_i), d_{ox}, L_o, W_o

Domain → / Parameters ↓	Weak inv.	strong inv.		
		$V_D = V_G$	$V_D > V_G$	$V_S \neq 0$
K	1,2,3			2,3
V_{TO}		4,5		
λ_1, λ_2		6,8	7,9	
B_o, Θ, E_C		6,8,10		10
b_h, a_w, b_w	1,3,11			
η	12			

Parameter extraction is only possible if reliable experimental data are available. Temperature has to be very stable during measurements, and a high degree of precision in the voltages and currents is necessary. A first set of parameters is obtained on the basis of the asymptotic relations. The final values are obtained by successive approximations and the use of the complete set of equations.

Some illustrative examples of the simulation capabilities of the CEMOS model are given below. The transistors were fabricated with the CEH silicon gate CMOS technology. Extracted parameters are given in appendix II.

Characteristics of $I = f(V_{GS}, V_{SB})$ are shown in fig. 15 for a fairly long (W/L = 20/22) n-channel MOSFET. These curves are used to extract the body factor $B_2 = K/\sqrt{U_{TH}}$ by means of 3 points at constant current at a low current level. The accuracy of the model is very good for $V_S = 0$ at all current levels. Substrate effect, especially the change in exponential slope as a function of V_S, is also correct. Slight deviations for the curves at $V_G = 0.5$ V and 2 V are attributed to non-uniform doping.

The fit is also excellent for $V_G = V_D$ in strong inversion. Mobility variation is properly taken into account also in presence of a substrate bias.

Characteristics $I = f(V_{DS})$ are shown in fig. 16 for the same n-channel MOSFET. Current increase and output conductance are fairly well described by the CEMOS model in strong inversion, but have a tendency to be larger than expected in weak inversion, especially for long n-channel MOSFETs (see fig. 16). We have found no explanation of this effect.

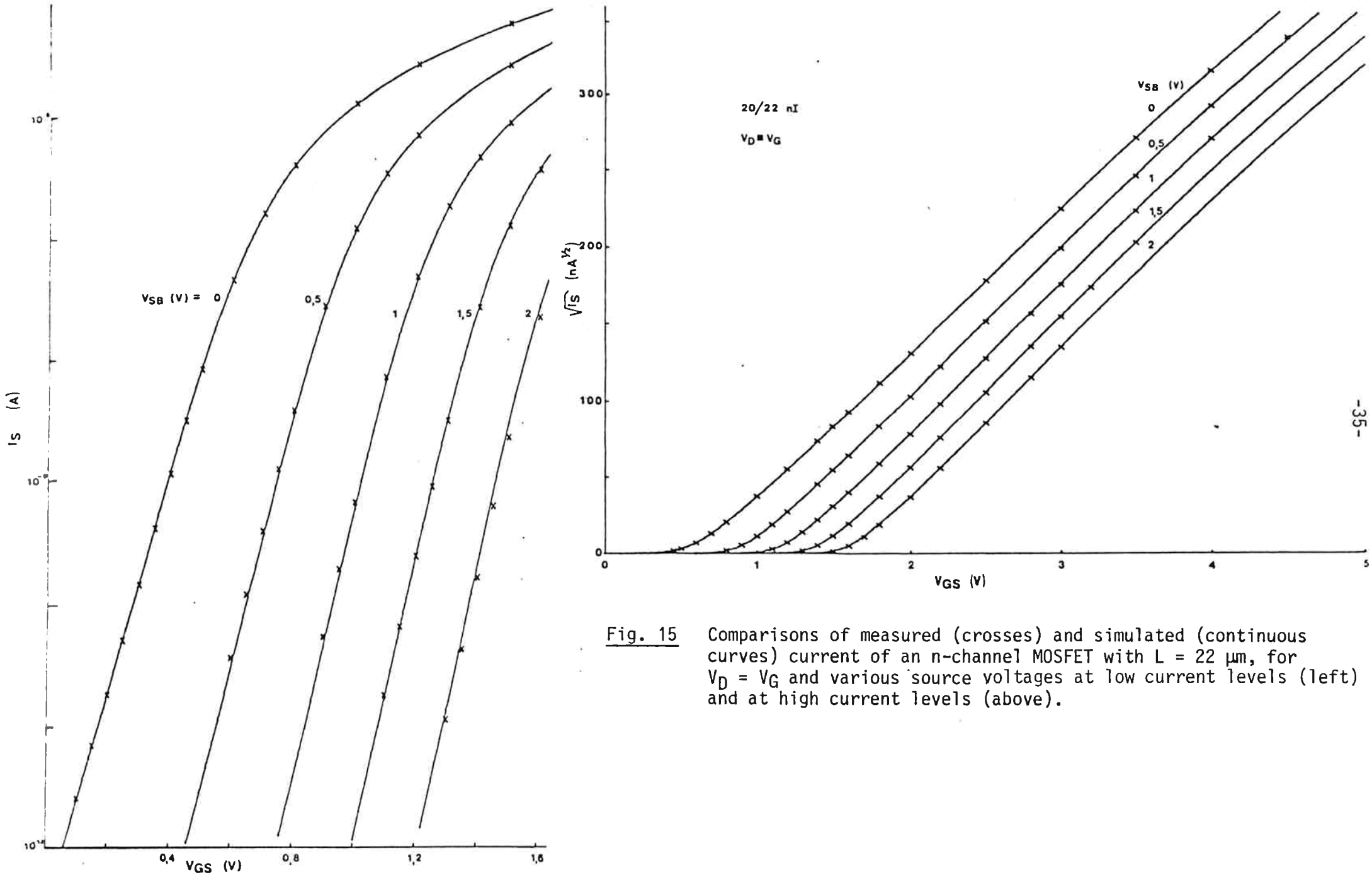

Fig. 15 Comparisons of measured (crosses) and simulated (continuous curves) current of an n-channel MOSFET with L = 22 µm, for $V_D = V_G$ and various source voltages at low current levels (left) and at high current levels (above).

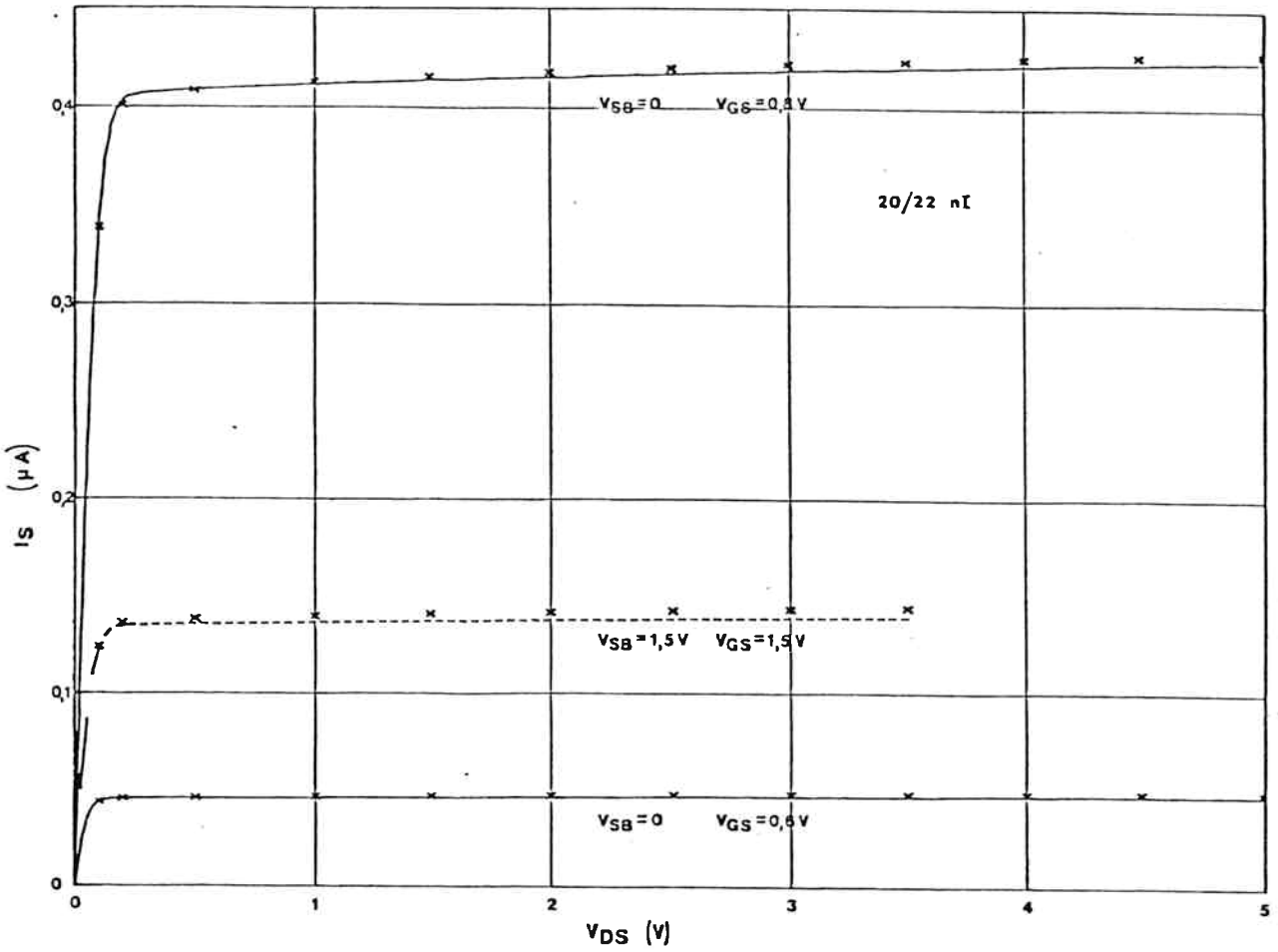

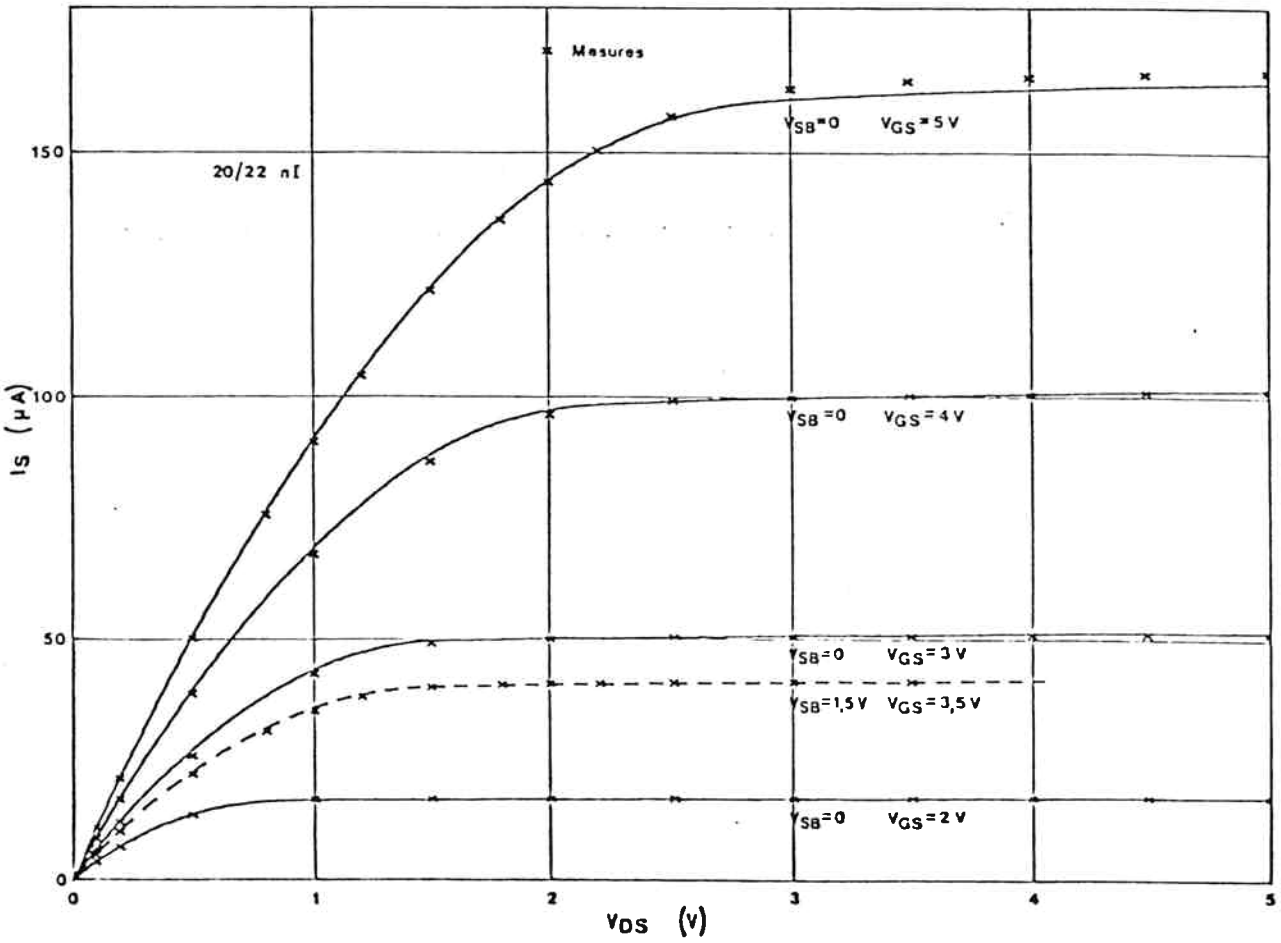

Fig. 16 Output characteristics for the same transistor as in fig. 15, at low current (top) and at high current (bottom).

Dimensional effects seem to give negligeable errors for effective channel lengths down to about 6 µm; an example is given in fig. 17 for a MOSFET with a channel length of 5.6 µm. Extension of the model down to $\simeq$ 2.5 µm is allowed with some systematic variations of the parameters and a reduced overall accuracy.

Samples with different oxide thicknesses (d_{ox} = 28 and 1000 nm) generally confirm the expectations: K, λ_1, B_o/b_h^2, n-m are proportional to d_{ox}; λ_2, Θ, a_w, b_w, K_w, η are independent of d_{ox} and finally a_h (=b_h) still obeys eq. (48), with B_2 deduced from K through (23).

Temperature effects on the first order parameters (V_{TO}, ϕ_F, B_o) conform very well with predictions based on the long channel model. λ_1 and $2a_w$ are found to vary somewhat with temperatures. K, Θ, λ_2, K_w, b_w/a_w and η show insignificant variations between -40 and +100°C.

Voltage limitations were arbitrarily chosen from the beginning with V_G, $V_D \leqslant 5$ V. The model is still useful up to $\sim$ 20 V with reduced accuracy or an improved expression of the mobility variation, as is known in other CAD programs. The true limitations in the accuracy of simulations should be considered carefully by taking into account all the surrounding elements of the MOSFET and the physical effects likely to occur: leakage currents in junctions, enhanced substrate current, parasitic channels, etc.

With the right choice of parameters, the overall accuracy of the model is better than 10%, and even a few % above V_T. The range of currents where this accuracy can be guaranteed extends over more than 8 decades.

Conclusions

A good method of modelling the static characteristics of MOSFETs consists to start with the long channel approximation, to express it with explicit formulas and to complete it with the most important corrections due to second order effects. Accuracy of a few percent is obtained over more than 8 decades of current from weak inversion to high current densities, and covering a wide range of technological variations. Its main limitations are caused by punch-trough and very short channel effects, for which the two-dimensional situation has to be considered.

The model has been successfully applied in a modified DOMOS simulation program [79 Do] and its implantation in other programs is in course.

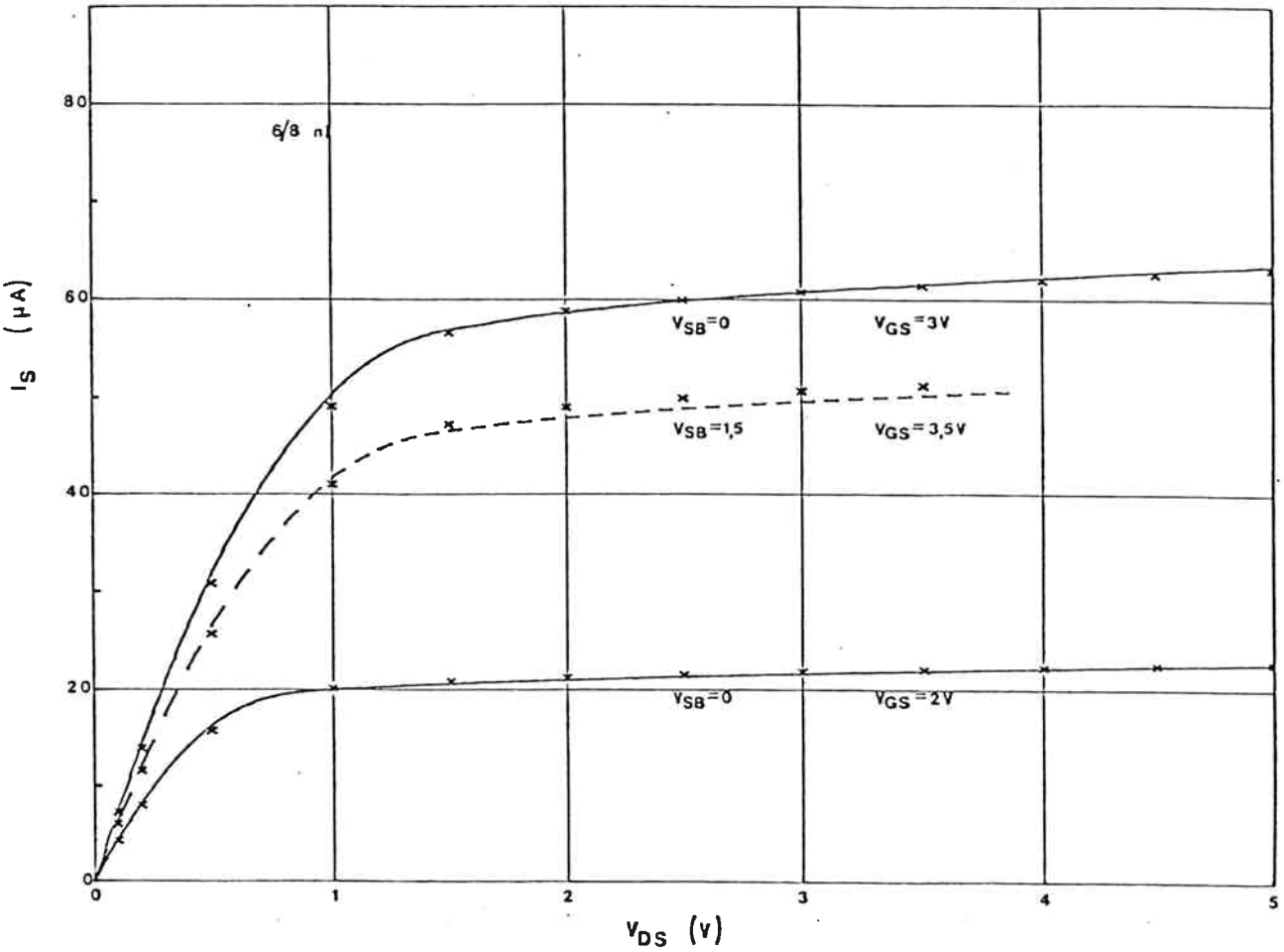

Fig. 17 Output characteristics of a shorter channel MOSFET (L_o = 5.6 μm).

The authors want to acknowledge the contributions of M. Dutoit and R. Zinszner for the implantation of the model in computer programs, and of F. Rahali for simulation on the PTIMOS program.

References

[64 Ih] H.K.J. Ihantola, J.L. Moll, "Design Theory of Surface Field-Effect Transistor", Solid-State Electronics, 1964, Vol. 7, pp. 423-430.

[66 Pa] H.C. Pao, C.T. Sah, "Effects of Diffusion Current on Characteristics of Metal-Oxide (Insulator)-Semiconductor Transistors", Solid-State Electronics, 1966, Vol. 9, pp. 927-937.

[66 Sa] C.T. Sah, H.C. Pao, "The Effects of Fixed Bulk Charge on the Characteristics of Metal-Oxide-Semiconductor Transistors", IEEE Trans. on Electron Devices, April 1966, ED-13, No 4, pp. 393-409.

[69 Sz] S.M. Sze, "Physics of Semiconductor Devices", Wiley 1969.

[71 Sh] J.M. Shannon, "D.C. Measurement of the Space Charge Capacitance and Impurity Profile beneath the Gate of an MOST", Solid-State Electronics, Nov. 1971, Vol. 14, No 11, pp. 1099-1106.

[72 Ba] M.B. Barron, "Low Level Currents in Insulated Gate Field Effect Transistors", Solid-State Electronics, March 1972, Vol. 15, No 3, pp. 293-302.

[72 Me] G. Merckel, J. Borel, N.Z. Cupcea, "An Accurate Large-Signal MOS Transistor Model for Use in Computer-Aided Design", IEEE Trans. on Electron Devices, May 1972, ED-19, No 5, pp. 681-690.

[72 Sw] R.M. Swanson, J.D. Meindl, "Ion Implanted Complementary MOS Transistors in Low-Voltage Circuits", IEEE J. of Solid-State Circuits, April 1972, SC-7, No 2, pp. 146-153.

[73 Ro] P. Rossel, "Propriétés statiques et dynamiques du transistor à effet de champ à grille isolée", Thèse No 529 Université Paul Sabatier de Toulouse, Mars 1973.

[74 Tr] R.R. Troutman, "Subthreshold Design Considerations for Insulated Gate Field Effect Transistors", IEEE J. of Solid-State Circuits, April 1974, SC-9, No 2, pp. 55-60.

[74 Ya] L.D. Yau, "A Simple Theory to Predict the Threshold Voltage of Short-Channel IGFET's", Solid-State Electronics, October 1974, Vol. 17, No 10, pp. 1059-1063.

[75 Sw] R.M. Swanson, J.D. Meindl, "Fundamental Performance Limits of MOST Integrated Circuits", 1975 IEEE Int. Solid-State Circuits Conference, Digest of Technical Papers, Vol. XVIII, pp. 110-111.

[77 Fu] M. Fukuma, M. Matsumura, "A Simple Model for Short Channel MOSFET's", Proceedings of the IEEE, August 1977, Vol. 65, No 8, pp. 1212-1213.

[77 Tr] R.R. Troutman, A.G. Fortino, "Simple Model for Threshold Voltage in a Short-Channel IGFET", IEEE Trans. on Electron Devices, October 1977, ED-24, No 10, pp. 1266-1268.

[77 Vi] E. Vittoz, J. Fellrath, "CMOS Analog Integrated Circuits Based on Weak Inversion Operation", IEEE J. of Solid-State Circuits, June 1977, SC-12, No 3, pp. 224-231.

[78 Br] J.R. Brews, "A Charge-Sheet Model of the MOSFET", Solid-State Electronics, February 1978, Vol. 21, No 2, pp. 345-355.

[78 Mu] P.A. Muls, G.J. Declerck, R.J. van Overstraeten, "Characterisation of the MOSFET Operating in Weak Inversion", in Advances in Electronics and Electron Physics, Vol. 47, edited by L. Marton, Academic Press 1978, pp. 197-266.

[78 Ta] G.W. Taylor, "Subthreshold Conduction in MOSFET's", IEEE Trans. on Electron Devices, March 1978, ED-25, No 3, pp. 337-350.

[79 DO] "DOMOS. Ein nichtlineares, dynamisches Simulations-und Optimierungsprogramm für integrierte MOS-Schaltungen. Version 7/2", Universität Dortmund, Lehrstuhl Bauelemente der Elektrotechnik, 30.1.1979.

[79 Ho] B. Hoefflinger, H. Sibbert, G. Zimmer, "Model and Performance of Hot-Electron MOS Transistors for VLSI", IEEE Trans. on Electron Devices, April 1979, ED-26, No 4, pp. 513-520.

[79 Ko] N. Kotani, S. Kawazu, "Computer Analysis of Punch-Through in MOSFET's", Solid-State Electronics, January 1979, Vol. 22, No 1, pp. 63-70.

[79 Ta] G.W. Taylor, "The Effects of Two-Dimensional Charge Sharing on the Above-Threshold Characteristics of Short-Channel IGFETS", Solid-State Electronics, August 1979, Vol. 22, No 8, pp. 701-717.

[79 Tr] R.R. Troutman, "VLSI Limitations from Drain-Induced Barrier Lowering", IEEE Trans. on Electron Devices, April 1979, ED-26, No 4, pp. 461-468.

[79 Wi] F. van de Wiele, "A Long-Channel MOSFET Model", Solid-State Electronics, Dec. 1979, Vol. 22, No 12, pp. 991-997.

[80 Ch] J.C.J. Chern, P. Chang, R.F. Motta, N. Godinho, "A New Method To Determine MOSFET Channel Length", IEEE Electron Device Letters, September 1980, EDL-1, No 9, pp. 170-173.

[80 Kl] F.M. Klaassen, W.C.J. de Groot, "Modelling of Scaled-Down MOS Transitors", Solid-State Electronics, 1980, Vol. 23, pp. 237-242.

[80 Li] S. Liu, B. Hoefflinger, D.O. Pederson, "Interactive Two-Dimensional Design of Barrier-Controlled MOS Transistors", IEEE Trans. on Electron Devices, August 1980, ED-27, No 8, pp. 1550-1558.

[80 Vl] A. Vladimirescu, S. Liu, "The Simulation of MOS Integrated Circuits Using SPICE 2", Memorandum No UCB/ERL M80/7, University of California, Berkeley, February 1980.

[81 Br] J.R. Brews, "Physics of the MOS Transistor", in Applied Solid-State Science, Supplement 2, Part A, Silicon Integrated Circuits, edited by D. Kahng, Academic Press, 1981, pp. 1-120.

[82 An] P. Antognetti, D.D. Caviglia, E. Profumo, "CAD Model for Threshold and Subthreshold Conduction in MOSFET's", IEEE J. of Solid-State Circuits, June 1982, SC-17, No 3, pp. 454-458.

[82 Fi] W. Fichtner, R.K. Watts, D.B. Fraser, R.L. Johnston, S.M. Sze, "0.15 µm Channel-Length MOSFET's Fabricated Using E-Beam Lithography", IEEE Electron Device Letters, December 1982, EDL-3, No 12, pp. 412-414.

[82 Ra] K.N. Ratnakumar, J.D. Meindl, "Short-Channel MOST Threshold Voltage Model", IEEE J. of Solid-State Circuits, October 1982, SC-17, No 5, pp. 937-948.

[82 Ya] P. Yang, P.K. Chatterjee, "SPICE Modeling for Small Geometry MOSFET Circuits", IEEE Trans. on Computer-Aided Design of Integrated Circuits and Systems, October 1982, CAD-1, No 4, pp. 169-182.

[83 Gu] P.P. Guebels, F. Van de Wiele, "A Small Geometry MOSFET Model for CAD Applications", Solid-State Electronics, April 1983, Vol. 26, No 4, pp. 267-273.

[83 Pi] R.F. Pierret, J.A. Shields, "Simplified Long-Channel MOSFET Theory", Solid-State Electronics, February 1983, Vol. 26, No 2, pp. 143-147.

[83 Si] M. Simard-Normandin, "Channel Length Dependence of the Body Factor Effect in NMOS Devices", IEEE Trans. on Computer-Aided Design of Integrated Circuits and Systems, January 1983, CAD-2, No 1, pp. 2-4.

HO/SC/mm
3.5.1983

Continuous Static Model of MOST for Analog Circuits

NOTATIONS

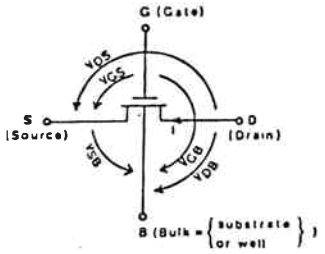

Signs: valid for n-channel
Change signs of V_{SB}, V_{GB}, V_{DB} and i for p-channel transistors ($V_{TO} > 0$)

Symb.	Unit	Explanation	Symb.	Unit	Explanation
a_w	-	numerical coeff.	q	As	electron charge
B	-	bulk (index)	S	-	source (index)
B	A/V^2	effective gain	T	°K	absolute temperature
B_0	A/V^2	initial eff. gain	U_{TH}	V	thermal voltage
b_h	-	numerical coeff.	V_{ij}	V	voltage between i and j
b_w	-	numerical coeff.	V_C	V	control voltage
C_{ox}	F/m^2	spec.gate capac.	V_{TO}	V	extrapol. threshold volt.
D	-	drain (index)	V_x	V	variable (V_{SB} or V_{DB})
d_{ox}	m	gate ox. thick.	W	m	layout channel width
E_C	V/m	critical longitud. field	W_0	m	eff. channel width
G	-	gate (index)	y	-	auxiliary function
g_D	A/V	output conductance	γ	-	control slope
g_m	A/V	transconductance	ΔL	m	channel length correct.
g_S	A/V	source conductance	ΔW	m	channel width correct.
i	A	channel current	ε_s	F/m	substrate permittivity
K_1	$V^{1/2}$	substrate effect	ε_{ox}	F/m	oxide permittivity
K_2	$V^{1/2}$	coeff. of depl. length	ξ	V/°K	temp. coeff. of V_{TO}
K_w	-	numerical coeff.	η	-	exponent (mobility)
l_{dep}	m	drain depl. length	Θ	V^{-1}	volt. coeff. (mobility)
L	m	layout channel length	λ_1	-	num. coeff. in l_{dep}
L_0	m	eff. ch. length below sat.	λ_2	-	num. coeff. in l_{dep}
N_B	m^{-3}	bulk doping conc.	μ_0	m^2/VS	initial mobility
n_i	m^{-3}	intr. carrier conc.	ϕ_F	V	Fermi potential

GENERAL EQUATIONS

Control voltage

$$V_C = V_{GB} - V_{TO} - K_1 \left[\sqrt{V_{GB} - V_{TO} + \left(\frac{K_1}{2} + \sqrt{2\,\phi_F}\right)^2} - \left(\frac{K_1}{2} + \sqrt{2\,\phi_F}\right) \right]$$

Control slope

$$\gamma = \frac{\partial V_C}{\partial V_{GB}} = 1 - \frac{K_1}{2\sqrt{V_{GB} - V_{TO} + \left(\frac{K_1}{2} + \sqrt{2\,\phi_F}\right)^2}}$$

Auxiliary function

$$y(V_x) = \ln^2 \left[1 + b_h \sqrt{2\,K_w} \exp \frac{a_w V_C - b_w V_x}{U_{TH}} + \exp\left(b_h \frac{V_C - V_x}{U_{TH}}\right) \right]$$

Depletion length

$$l_{dep} = \lambda_2 K_2 \sqrt{\frac{V_{DB} - V_C + U_{TH}\sqrt{y(V_{DB})} / b_h}{1 + \lambda_1\, y\,(V_{SB})}}$$

Eff. ch. length below sat.

$$L_0 = L - \Delta L$$

Eff. channel width

$$W_0 = W + \Delta W$$

Initial effective gain

$$B_0 = 2\, b_h^2\, \mu_0\, C_{ox} \frac{W_0}{L_0}$$

Effective gain

$$B = \frac{B_0}{(1 + \Theta V_C)\left(1 + \frac{V_C - V_{SB} - U_{TH}\sqrt{y(V_{DB})} / b_h}{E_C L_0}\right)\left(1 - \frac{l_{dep}}{L_0}\right)}$$

Channel current

$$i = \frac{B}{2\, b_h^2}\, U_{TH}^2 \left[y\,(V_{SB}) - y\,(V_{DB}) \right]$$

PHYSICAL RELATIONS

Coefficients : $K_1 = \frac{\sqrt{2\ \varepsilon_s\ q\ N_B}}{C_{ox}}$; $K_2 = \sqrt{\frac{2\ \varepsilon_s}{q\ N_B}}$;

Fermi potential : $\phi_F = U_{TH} \ln \frac{N_B}{n_i}$; specific gate capacitance: $C_{ox} = \frac{\varepsilon_{ox}}{d_{ox}}$

Temperature effects : $T(°K) = T(°C) + 273.15$; $U_{TH} = \frac{T}{11610}$; $V_{TO}(T) = V_{TO}(T_0) + \xi\,(T - T_0)$

$n_i(m^{-3}) = 3.8 \times 10^{22} \times T^{3/2} \times \exp(-7000/T)$; $\mu_0(T) = \mu_0(T_0) \cdot (\frac{T_0}{T})^?$

Constants : $\varepsilon_s = 1.045 \times 10^{-10}$ F/m ; $\varepsilon_{ox} = 0.345 \times 10^{-10}$ F/m ; $q = 1.602\ 10^{-19}$ As

Technology dependent constants: see 2.2.1/1.4

APPROXIMATIONS FOR HAND CALCULATIONS

Simplifications: $a_w = b_w = 0.5$

Supplementary terms in g_D, g_s and g_m expressions due to $1/E_C \neq 0$ and $\lambda_1 \neq 0$ were neglected (they are negligible for $L_0 \gtrsim 6$ µm).

Assumptions / Variable	weak inversion $V_C < V_{SB} - 0.1$ V		strong inversion $V_C > V_{SB} + 0.3$ V	
	below saturation $V_{DS} < 0.1$ V	saturation $V_{DS} > 0.2$ V	below saturation $V_{DB} < V_C - 0.1$ V	saturation $V_{DB} > V_C + 0.1$ V
i	$K_w B U_{TH}^2 \exp\left(\frac{V_C - V_{SB}}{U_{TH}}\right)\left[1 - \exp\left(-\frac{V_{DS}}{U_{TH}}\right)\right]$	$K_w B U_{TH}^2 \exp\left(\frac{V_C - V_{SB}}{U_{TH}}\right)$	$B\ V_{DS}\left(V_C - V_{SB} - \frac{V_{DS}}{2}\right)$	$\frac{1}{2} B\ (V_C - V_{SB})^2$
l_{dep}	—	$\lambda_2 K_2 \sqrt{V_{DB} - V_C}$	0	$\lambda_2 K_2 \sqrt{\frac{V_{DB} - V_C}{1 + \lambda_1 [b_h (V_C - V_{SB})/U_{TH}]^2}}$
$\frac{B_0}{B}$	1	$1 - \frac{l_{dep}}{L_0}$	$(1 + \Theta V_C)\left(1 + \frac{V_{DS}}{E_C L_0}\right)$	$\left(1 - \frac{l_{dep}}{L_0}\right)(1 + \Theta V_C)\left(1 + \frac{V_C - V_{SB}}{E_C L_0}\right)$
$g_D = \frac{\partial i}{\partial V_{DB}}$	$\frac{i}{U_{TH}} \frac{1}{\exp(V_{DS}/U_{TH}) - 1}$	$\frac{1}{2} \frac{l_{dep}}{L_0 - l_{dep}} \frac{i}{V_{DB} - V_C}$	$B\ (V_C - V_{DB})$	$\frac{1}{2} \frac{l_{dep}}{L_0 - l_{dep}} \frac{i}{V_{DB} - V_C}$
$g_s = \frac{\partial i}{\partial V_{SB}}$	$-\frac{i}{U_{TH}} \frac{1}{1 - \exp(-V_{DS}/U_{TH})}$	$-\frac{i}{U_{TH}}$	$-B\ (V_C - V_{SB})$	$-B\ (V_C - V_{SB})$
$g_m = \frac{\partial i}{\partial V_{GB}}$	$\gamma \frac{i}{U_{TH}}$	$\gamma \frac{i}{U_{TH}}$	$\gamma B V_{DS}\left[1 - \Theta\left(V_C - V_{SB} - \frac{V_{DS}}{2}\right)\right]$	$\gamma B (V_C - V_{SB})\left[1 - \frac{V_C - V_{SB}}{2}\left(\Theta + \frac{g_D}{i}\right)\right]$

Numerical values to be inserted in CEMOS model (see 2.2.1/1.3).

Values at room temperature (T = 25°C).

Symbol	Unit	Comments	p-channel min.	p-channel typ.	p-channel max.	n-channel min.	n-channel typ.	n-channel max.
V_{T0}	V	Extrapolated threshold [1]	0.30	0.45	0.60	0.40	0.55	0.70
ξ	V/°K	Threshold temper.coefficient [4]	0	-1.6×10^{-3}	-3×10^{-3}	0	-1.6×10^{-3}	-3×10^{-3}
N_B	m^{-3}	Bulk concentration	1.8×10^{21}	2×10^{21}	2.2×10^{21}	4.5×10^{21}	5.5×10^{21}	6.5×10^{21}
C_{ox}	$\mu F/m^2$	Gate capacitance	317	345	373	317	345	373
K_1	$V^{1/2}$	Bulk effect	0.66	0.75	0.85	1.04	1.24	1.47
ϕ_F	V	Fermi potential	0.305	0.308	0.310	0.329	0.334	0.338
$\frac{K_1}{2}+\sqrt{2\phi_F}$	$V^{1/2}$	Expression intervening in V_C	1.11	1.16	1.21	1.33	1.44	1.56
b_h	-	Coefficient [2]	0.75	0.76	0.77	0.80	0.82	0.84
a_w	-	Coefficient [4]	0.46	0.47	0.5	0.48	0.50	0.5
b_w	-	Coefficient [4]	0.46	0.48	0.5	0.48	0.49	0.5
K_w	-	Coefficient	1	2.5	4	1	2.5	4
$\lambda_1 L_0$	µm	Coefficient in l_{dep} [4]	0	0	1×10^{-3}	0	1.2×10^{-3}	2×10^{-3}
$\lambda_2 K_2$	$\mu m/V^{1/2}$	Coefficient in l_{dep} [3]	0.4	0.54	0.8	0.3	0.42	0.6
μ_0	m^2/Vs	Initial mobility	0.025	0.029	0.033	0.09	0.10	0.11
η	-	Exponent in mobility	1.5	1.5	2	1.5	1.5	2
Θ	V^{-1}	Voltage coefficient in mobility	0.1	0.125	0.15	0.1	0.125	0.15
$1/E_C$	µm/V	Inverse of longitudinal field [4]	0	0	0.2	0	0.22	0.5
$B_0\frac{L_0}{W_0}$	$\mu A/V^2$	Initial gain (V_C, V_D low)	8.9	11.6	14,6	36	46	58
ΔW	µm	Channel width correction	-0.4	1.2	1,5	-0.4	1.2	1.4
ΔL	µm	Channel length correction	2.2	2.4	3.4	2.0	2.4	3.2

1) As V_{T0} varies with the length of transistors, higher (n-channel) or smaller (p-channel) values might occur for very long transistors ($L_0 \gg 50$ µm).

2) This parameter is estimated with the following approximate theoretical expression: $b_h = 0.678 + 0.018\ K_1/\sqrt{U_{TH}}$.

3) For long ($L_0 \gg 20$ µm) n-channel transistors below the strong inversion, $\lambda_2 K_2$ might be higher.

4) Some extreme values ($\xi = 0$; $a_w = 0.5$; $b_w = 0.5$: $\lambda_1 = 0$ and $1/E_C = 0$) were introduced in order to allow the use of simplified expressions.

 To be presented at NASECODE III, Galway, 15-17 June 1983

AN ACCURATE 2-D SIMULATION PROGRAM OF MOS TRANSISTORS USING THE FINITE ELEMENT METHOD, AND INTERFACED TO OTHER PROCESS SIMULATION PROGRAMS

F. RAHALI
ELECTRONICS LABOTATORY OF THE SWISS FEDERAL INSTITUTE OF TECHNOLOGY, LAUSANNE

Abstract

We describe a new computer program, PTIMOS, for designing short-channel MOS transistors (MOST). This program is based on the finite element method, which has several advantages over the classical finite difference method. A careful choice of algorithms has allowed us to obtain good numerical stability, very accurate electrical characteristics, and to minimize computer memory and execution time. Input format is very easy to learn. Interfaces with process modeling programs and measured data files have been included. These features make our program a very efficient tool as demonstrated on several practical examples drawn from a 2 micron CMOS technology.

1. Introduction

The development of integrated circuits with micron-size devices requires powerful computer programs to optimize process and device parameters. In order to be helpful to engineers, such programs need to be user-friendly and employ available computer resources efficiently. They should not only be easy to run, but should also interface to data generated by external means, i.e. process modeling programs or measured data.

Here, we are concerned with the optimal design of n- and p-channel MOS transistors (MOST) for a 2 micron CMOS technology. Several computer programs already exist that solve the two-dimensional electrostatic problem presented by such devices [1]. Nearly all of them are based on the finite difference method. The finite element method, on the other hand, has several advantages, such as more flexible mesh generation and easier formulation of boundary conditions. Charge and current conservation are automatically satisfied.

We present a new computer program, PTIMOS, that takes advantage of these improvements. Particular care has been given to develop algorithms that insure numerical stability, and minimize computer memory and execution time. The program features an input format that is easily grasped as well as painless interfacing to data files generated by SUPREM [2], NEWDIF [3], or measurements.

Various parameters of the simple analytical, long-channel model, such as threshold voltage, transconductance or subthreshold slope, are automatically calculated, when applicable.

Detailed comparisons between calculated and measured characteristics of actual MOSTs illustrate the efficiency and accuracy of this new program. We show the importance of starting with the correct doping profiles by using both calculated and measured profiles which differ significantly.

2. Physical model

Since the calculation of two-dimensional electrical potential, charge carrier and current distributions in a MOST is a well-Known problem [4], we will be very sketchy.

The main assumptions are :

. the semiconductor is non degenerate
. the impurities are completely ionized
. the temperature is constant within the device
. Einstein's relation is always valid
. Boltzmann's statistics is valid on the contacts

The behavior of semiconductor devices is described by 3 differential equations:

. Poisson's equation

$$\text{div}\ (\varepsilon\ \vec{\text{grad}}\ V) = q\ (n-p+N_A-N_D) \qquad (1)$$

. the continuity equation for electrons

$$\frac{\partial n}{\partial t} = -\ R + \frac{1}{q}\ \text{div}\ (-q\mu_n n\ \vec{\text{grad}}\ V + qD_n\ \vec{\text{grad}}\ n) \qquad (2)$$

. the continuity equation for holes

$$\frac{\partial p}{\partial t} = -\ R + \frac{1}{q}\ \text{div}\ (\ q\mu_p p\ \vec{\text{grad}}\ V + qD_p\ \vec{\text{grad}}\ p) \qquad (3)$$

For the D.C. problem, $\frac{\partial n}{\partial t}$ and $\frac{\partial p}{\partial t}$ are zero.

The symbols are defined as:

- V : potential
- n : electron density
- p : hole density
- N_A : acceptor carrier density
- N_D : donor carrier density
- q : elementary charge
- ε : permittivity

μ_n : electron mobility
μ_p : hole mobility
D_n : electron diffusion parameter
D_p : hole diffusion parameter
R : recombination rate

The mobilities are assumed to be dependent on the doping profile and the normal and lateral electric fields. The model used is simple but sufficient enough. We have modified the one proposed by K.YAMAGUCHI [5] to have a maximum accuracy on the electrical characteristics. The best results were obtained with:

$$\mu = \mu_o / \sqrt{f(E_{//})+g(E_\perp)-1} \quad (4)$$

$$f(E_{//}) = 1 + \frac{(E_{//}/A)^2}{(E_{//}/A)+F} + (E_{//}/B)^2 + \frac{N_B}{(N_B/S)+N} \quad (5)$$

$$g(E_\perp) = 1 + \alpha E_\perp \quad (6)$$

where $E_{//}$ and $E_\perp$ are the lateral and normal fields, N_B is the impurity concentration and μ_o, A, B, S, N, α are constants.

For the solution of the majority carrier equation (holes for an n-channel MOST and electrons for a p-channel MOST), we have assumed that no current is due to these carriers.

3. Numerical model

To solve the 3 coupled differential equations, we preferred to use a fixed point method rather than Newton's method, because it minimizes computer memory, and each equation is solved sequentially.

Poisson's equation is linearized by Gummel's algorithm [6] with overrelaxation on the potential.

The continuity equations are best solved after a change of variables that transform them into elliptical differential equations. We write:

$$n = n_i \lambda \exp(qV/KT) \quad (7)$$

$$p = n_i \mu \exp(-qV/KT) \quad (8)$$

and take λ and μ as the new independant variables. This transformation yields better numerical stability. Since we assume that there is no current due to majority carriers, the continuity equation reduces to the simple form:

μ = constant

To discretize the differential equations we use linear finite elements. Their configuration is chosen so as to obtain band matrices without having

to sacrifice any mesh points (Fig.1). The mesh is automatically generated once the doping profiles and the applied biases are specified. Within each element the current density is held constant in the source-drain direction and allowed to vary exponentially perpendicularly to the gate. This increases significantly the accuracy of the solution.

The linearized Poisson's equation is easily solved by any method. We chose an incomplete Cholesky decomposition because it converges more rapidly.

For the continuity equation, the change of variables introduced previously leaves one with rapidly varying exponential terms. Therefore the rigidity matrix has to be preconditionned prior to solving the set of linear equations again by an incomplete Cholesky decomposition. Calculations are stopped once the difference between the current at the source and the drain amounts to less than 0.5% during 3 successive iterations.

Since there is no current flowing across the Si/SiO_2 interface, one expects intuitively that λ should be one-dimensional in the channel. This is indeed verified numerically. In most cases, the current varies by less than 1% if one pursues the solution in 2 dimensions.

4. Threshold voltage

For a specified bulk bias, PTIMOS calculates the threshold voltage V_{th} without having to simulate a complete I-V characteristic. We define V_{th} as the gate bias that produces a surface density of minority carriers in the middle of the channel equal to the average dopant concentration in the depleted layer for $V_{DS} = 0$. The program calculates two values for V_{th}, one by neglecting the influence of source and drain depletion layers (1d case), the other with the full 2d solution. For the long-channel case, we obtain good agreement with the standard formula. For short channels, V_{th} coincides with the value extrapolated from the transfer characteristics with small V_{DS}. The cost of this calculation is less than that of one operating point.

5. Comparison of simulated and experimental results

We show results on a p-channel MOST with ion implanted channel [7].

The only fitted parameter is the flat-band voltage V_{fb}. The reason is that for a non-uniform profile, V_{fb} deduced from a high frequency C-V curve is an effective value that includes fixed interface charges as well as the doping profile. For the solution of Poisson's equation, only the part due to fixed charges is needed. We obtain V_{fb} by shifting the calculated transfer characteristics in the subthreshold region along the voltage axis to make it

coincide with the measured one.

The electrical characteristics were simulated both with the doping profiles calculated by SUPREM and with the ones measured by the pulsed C-V (channel, see Fig.2) and spreading (source-drain) resistance methods. (Figs.3,4,5,6). Better agreement is obtained with the latter. This shows the need for precise process modeling in order to achieve correct results. The simulated and measured MOST was a 2 micron p-channel with 0.5 micron junction depth.

We get similar results for n-channel MOSTs.

6. References

[1] S.Selberherr, W.Fichtner and H.W.Pötzl, A program package to facilitate MOS device design and analysis, NASECODE I, Dublin, June 1978.

[2] D.A.Antoniadis, S.E.Hansen and R.W.Dutton, SUPREM II - A program for IC process modeling and simulation, Technical Report - Stanford University, June 1978.

[3] To be published.

[4] M.Heydemann, Résolution numérique des équations bidimensionnelles de transport dans les semiconducteurs, Ph.D. thesis, Paris-Sud University, 1972.

[5] K.Yamaguchi, Field-dependant mobility model for two-dimensional numerical analysis of MOSFET's, IEEE Trans. Electron Devices, ED-26, 1068 (1979).

[6] H.K.Gummel, A self consistent iterative scheme for one-dimensional steady state transistor calculations, IEEE Trans. Electron Devices, ED-11, 455 (1964).

[7] P.Schwob, M.Dutoit, H.Luginbühl, J.C.Martin, M.Pfister, M.Gansner and M.Ilegems, A 2 micron silicon-gate CMOS technology for a static 1.5V 1 Kbit RAM, ESSDERC'80, York, September 15-18, 1980 and Journées d'électronique et de microtechnique 80, Lausanne, 7-9 octobre 1980.

[8] J.H.Hohl, Variational principles for semiconductor device modeling with finite element, IBM J.RES.DEVELOP. vol.22, No.2, March 1978.

[9] J.J.Barnes, R.J.Lomax, Finite element simulation of GaAs MESFET's with lateral doping profiles and submicron gates, IEEE Trans. Electron Devices, ED-23, No.9 (1976).

[10] F.Rahali, Analyse numérique à 2 dimensions de transistors MOS par la méthode des éléments finis, Technical Report - LEG 81.04, Swiss Federal Institute of Technology, Lausanne, Sept. 1981.

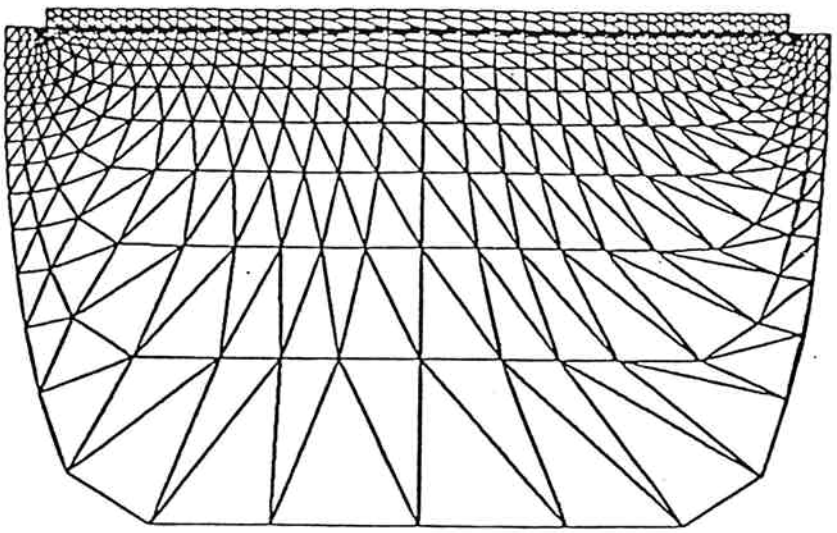

Fig. 1 Example of automatic mesh generated by PTIMOS

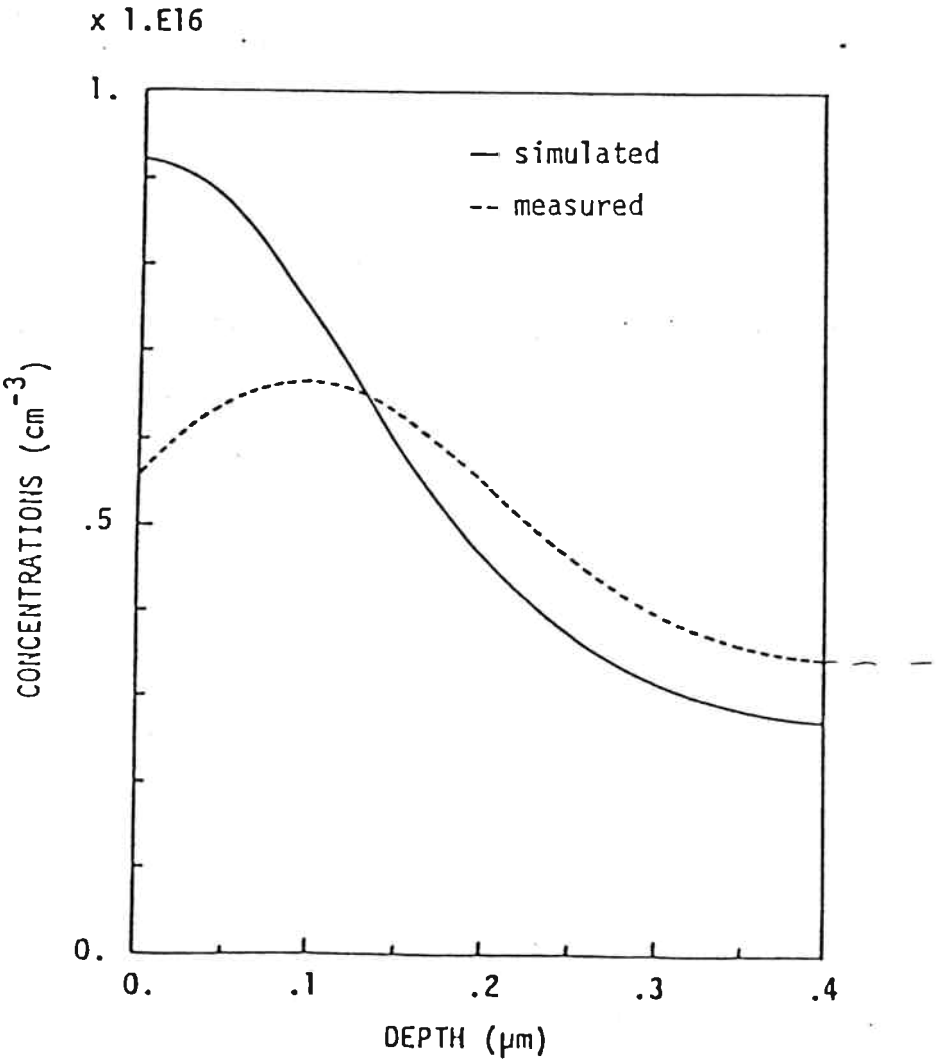

Fig. 2 Simulated (SUPREM II) and measured doping profiles (C-V method) in the channel

Electrical characteristics

– measurements on several chips.

• simulated with measured doping profiles and PTIMOS.

o simulated with SUPREM II and PTIMOS.

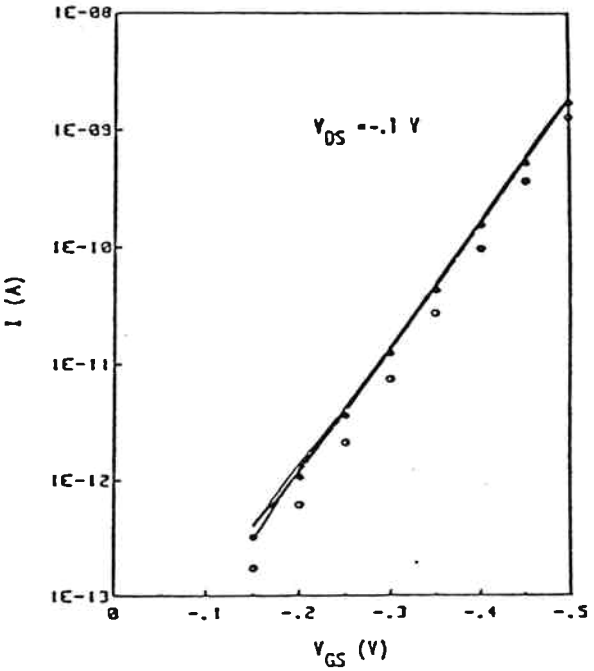

Fig. 3 Transfer characteristic in weak inversion.

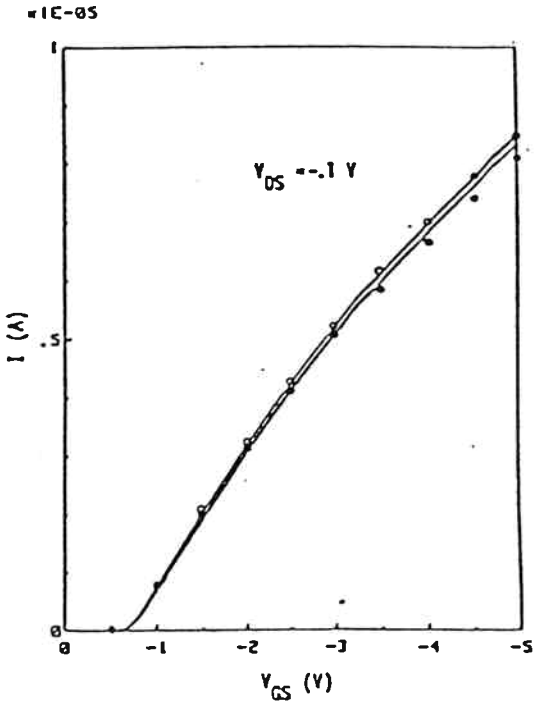

Fig. 4 Transfer characteristic in strong inversion. Triode regic

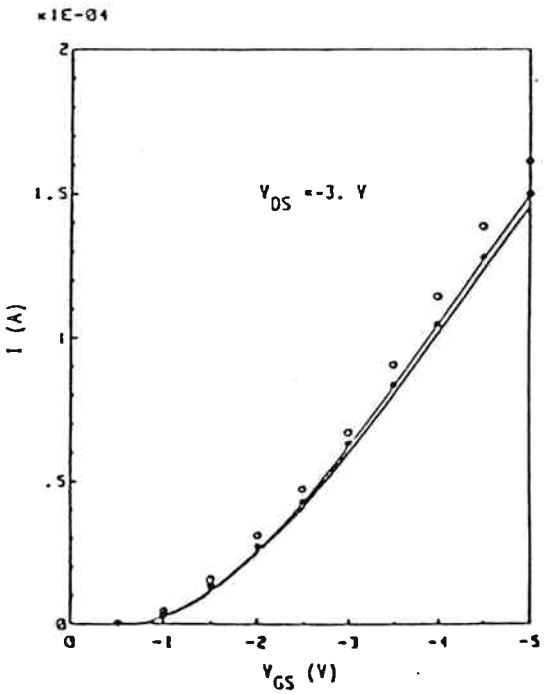

Fig. 5 Transfer characteristic in strong inversion.
Saturation region.

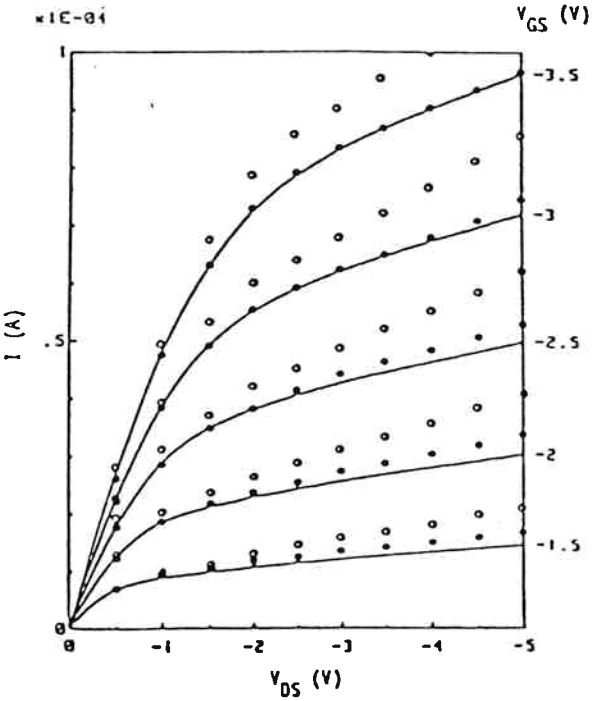

Fig. 6 Output characteristics.